JOURNAL OF GEOPHYSICAL RESEARCH, VOL. 105, NO. A12, PAGES 27,323–27,341, DECEMBER 1, 2000

Model for the partition of temperature between electrons and ions across collisionless, fast mode shocks

A. J. Hull[1] and J. D. Scudder
Department of Physics and Astronomy, University of Iowa, Iowa City

Abstract. The partition of temperature between electrons and ions across Earth's bow shock is a long-standing problem in modeling particle entry into the magnetosphere. Observations have shown that the ion temperature increase across collisionless, fast mode shocks (as in Earth's bow shock) is substantially larger than that of the electrons. A model that can quantitatively explain this result will provide a better understanding of the relationships between collisionless shock parameters and particle behavior across the shock layer, finding applications to multifluid models of particle entry to the Earth's magnetosphere, as in the polar rain. In this paper we present a model that quantitatively determines the partition of temperature between the electrons and ions across the shock. The model couples a simplified Vlasov guiding center ordered electron fluid problem with the Rankine-Hugoniot conservation equations to determine the downstream partition of electron and ion temperature given a few observational constraints. We work in the deHoffmann-Teller reference Frame (HTF) because in HTF the electrons are only coupled to the ions through the electrostatic potential. This approach does not preclude the subsequent secondary thermalization of the ions by means of wave-particle interactions. We demonstrate under this approximation that the model recovers the electron temperature jumps of a new ISEE 1 database of 129 Earth bow shock crossings developed and analyzed by *Hull et al.* [2000]. The model also recovers trends in the downstream ion temperature at shocks observed by ISEE 1 previously cataloged by *Thomsen et al.* [1987].

1. Introduction

Measurements [e.g., *Montgomery et al.*, 1970; *Scudder et al.*, 1973; *Feldman*, 1985; *Schwartz et al.*, 1988] have shown that although the plasma temperature increases across collisionless, fast mode shocks, the ion temperature increase is substantially larger than that of the electrons (electrons receive ~25% of the total available random energy). These trends have been observed at both strong and weak shocks with the differences in the electron and ion temperature jumps being more pronounced at shocks of greater strengths. An outstanding problem of collisionless shock physics is a quantitative determination of the postshocked partition of temperature between electrons and ions. One-fluid conservation of mass, momentum, and energy determine the total random energy available to the plasma as a whole but can not determine how much gets partitioned to the separate electron and ion components. Several mechanisms were proposed to explain the observed particle heating signatures [e.g., *Sagdeev*, 1966; *Biskamp*, 1973; *Leroy et al.*, 1982; *Paschmann et al.*, 1982; *Sckopke et al.*, 1983, 1990; *Wu et al.*, 1984; *Goodrich and Scudder*, 1984; *Feldman*, 1985; *Gosling and Robson*, 1985; *Winske et al.*, 1985; *Scudder*, 1995; *Krauss-Varban et al.*, 1995; *Balikhin et al.*, 1998]. However, no model for collisionless, fast mode shocks has been able to predict the full range of observed changes in electron and ion temperature which is the topic of this paper.

Analyses of high time resolution field and ion observations [*Paschmann et al.*, 1982; *Sckopke et al.*, 1983, 1990; *Gosling and Robson*, 1985] along with particle simulations using detailed diagnostics [*Leroy et al.*, 1982; *Leroy and Winske*, 1983; *Goodrich*, 1985; *Burgess et al.*, 1989; *Wilkinson*, 1991] have resulted in the present understanding that the ion temperature increase at strong and weak quasi-perpendicular shocks is a process initiated by the coherent Lorentz forces within the shock ramp followed by subsequent thermalization via waves farther downstream. With the ions being unmagnetized across the embedded DC electric and magnetic field, this heating process is a finite Larmor radius effect. Most of the supersonic ions are directly transmit-

[1]Now at the Space Science Laboratory, University of California, Berkeley.

Paper number 2000JA900105.
0148-0227/00/2000JA900105$09.00

ted, being slowed down and heated by the cross-shock potential. A small, gyrophase-selected fraction of the ion population ($\lesssim 20\%$ depending on shock strength) is specularly reflected by the shock macroscopic electric and magnetic fields. At quasi-perpendicular shocks, the reflected ions gyrate back to the shock layer after gaining energy by drifting along the electric field tangent to the shock surface, and the reflected ions subsequently traverse the shock layer. Studies suggest that the gross deformation of the ion velocity distribution function associated with the specular reflection process accounts for a substantial fraction of the total ion temperature increase occurring across supercritical, quasi-perpendicular shocks [e.g., *Gosling and Robson*, 1985, and references therein]. Wave-particle effects are thought to reduce free energy sources induced by the macroscopic fields and enhance the ion temperature as the ions convect farther downstream [*McKean et al.*, 1995]. These irreversible temperature changes are small compared to the bulk temperature changes caused by the coherent forces within the shock layer.

Coherent aspects of electron temperature changes have also received attention over the years. *Goodrich and Scudder* [1984] suggested that electron energization and hence the fluid electron temperature increase at collisionless shocks can be explained by the adiabatic motion of electrons in the shock DC electromagnetic forces. This coherent electron energization process is essentially a competition between the energy gained by the embedded cross-shock potential and the energy lost via the work done against the motional electric field in traversing the shock layer. The study by *Goodrich and Scudder* [1984] suggests that electron energization and hence temperature change are best viewed as a coherent process in the deHoffmann-Teller reference frame (HTF). The HTF is that special frame of reference in which the motional electric field vanishes. As a result, the HTF center of mass velocity and the magnetic field vector are parallel on both the preshocked (upstream) and postshocked (downstream) sides of the shock. A corollary to the HTF theorem is that the electron bulk velocity is approximately field-aligned inside the current-carrying layer provided that corrections that depend on electron anisotropy, inertia, and resistivity can be neglected [*Scudder*, 1987]. Electron energetics is much simpler in HTF because the electrons only gain the cross-shock electrostatic potential $\Delta\Phi^{HT}$ in crossing the layer.

The typical shock length scales documented by multiple spacecraft (S/C) across Earth's bow shock [*Russell et al.*, 1982; *Scudder et al.*, 1986b; *Newbury et al.*, 1998] or seen in simulations [e.g., *Leroy et al.*, 1982; *Savoini and Lembege*, 1994] suggest that the typical electron is magnetized in traversing the shock layer. With this in mind, *Scudder et al.* [1986c] exploited conservation of electron energy and magnetic moment constraints to demonstrate via a Vlasov-Liouville (V-L) mapping that the HTF potential is responsible for the lowest-order broadening of the electron distribution function parallel to the magnetic field, providing a possible explanation for the electron temperature increase across collisionless shocks. Wave-particle effects, although required, were found to provide secondary irreversible changes to the electron distribution function by "cooling" over inflated electron distributions. Other aspects of the V-L mapping technique have been employed to estimate $\Delta\Phi^{HT}$ across fast [*Schwartz et al.*, 1988] and slow mode shocks [*Schwartz et al.*, 1987] using just a piece of the electron distribution function. Recent studies [*Scudder*, 1995; *Hull et al.*, 1998] employed the V-L approach using model electron distributions to illustrate the effects of the shock macroscopic fields on magnetized electrons, and hence these studies verified the claims of *Scudder et al.* [1986c] at all pitch angles. In particular, the preferential perpendicular inflation signatures observed at weak shocks [*Feldman et al.*, 1983b], as well as the nearly isotropic inflation signatures observed at strong shocks [*Montgomery et al.*, 1970; *Scudder et al.*, 1973, 1986a; *Feldman et al.*, 1983a], are recovered by the V-L mapping procedure [*Scudder*, 1995; *Hull et al.*, 1998] without invoking wave-particle effects.

Despite the understanding that plasma temperature changes at fast mode shocks are primarily the result of coherent processes, a model that can predict the partition of electron and ion temperature within the coherent energization framework still remains to be developed. In this paper a model for the partition of temperature across collisionless, fast mode shocks is presented. A theoretical model which follows the details of both the electron and ion behavior across the layer is difficult to develop, because plasma phenomena at shocks occur over a wide range of length and time scales. Such an approach is not needed, since the change in the total pressure is guaranteed by the one-fluid conservation laws and the partition of pressure can be determined by determining either the electron or ion pressure change across the shock.

Because ion behavior is more complex, our approach is to develop an approximate multilevel theoretical model that takes advantage of the much simpler adiabatic electron behavior in HTF. The multilevel model couples a Vlasov guiding center ordered electron fluid problem with the Rankine-Hugoniot (RH) conservation equations to determine the downstream electron and ion temperature given a few observational constraints. The electron Vlasov problem determines the downstream electron pressure and temperature, whereas the ion pressure and temperature are determined by subtracting the more tractable electron pressure from the total pressure predicted by the one-fluid MHD conservation constraints. In HTF the model assumes that the electrons are coupled to the ions only through the electrostatic potential (e.g., there is no exchange of energy and momentum between electrons and ions via wave-particle interactions). The model's emphasis on the guiding center ordered electron behavior does not pre-

clude the effects of the locally produced waves on the ion thermalization process, for all the effects of the waves are included in the measured ion fluid quantities which when combined with those of the electrons determine the shock one-fluid conservation laws we seek to enforce and exploit in this paper. Under this approximation we show, for the first time, that the model recovers electron and ion temperature changes consistent with a broad range of shock observations.

The geometry and asymptotic states of 129 Earth bow shock crossings observed by ISEE 1 used in this study have been previously developed and characterized in a recent study [*Hull et al.*, 2000] by least squares fits to a subset of the RH equations via the method of *Viñas and Scudder* [1986]. A subset of the shock events have ion temperatures adapted from *Thomsen et al.* [1987].

The paper is organized as follows. In section 2 an overview of the approximate hybrid model (Vlasov electrons coupled with MHD) is presented. The electron Vlasov problem is discussed in section 2.1. Section 2.2 presents the model boundary electron velocity distribution functions used. The model assumptions are summarized in section 2.3. The solution scheme for the shape parameters that define f_1 and f_2 is discussed in section 2.4. The model predictions on ΔT_e and ΔT_i are compared to observations in sections 3 and 5, respectively. In section 4 we discuss the model's prediction for the scaling of the empirically suggested κ parameter [*Hull et al.*, 2000], which relates the HTF potential increments to the magnetic field increments through the shock. section 6 describes the development of a one-sided predictive model based on what we have learned from the two-point problem. Conclusions are presented in section 7.

2. Model

The multilevel model can be organized into five steps to be followed in order to obtain the downstream electron and ion temperature. An overview of the solution scheme of the model is given in Figure 1. In step 1 we use *Whang*'s [1987] formulation of the RH relations to solve for the downstream total pressure P_2, plasma density N_2, and magnetic field intensity B_2 given the upstream plasma density N_1, shock rest frame plasma bulk speed U_{n1} along the shock normal, total plasma pressure P_1, magnetic field intensity B_1, and the angle θ_{Bn1} between the shock normal and magnetic field vector. In step 2 the steady state electron Vlasov equation is solved by the method of characteristics in the adiabatic approximation using prescribed fields [e.g., *Scudder et al.*, 1986c; *Scudder*, 1995; *Hull et al.*, 1998]. A well-posed Vlasov treatment requires a choice of the upstream and downstream boundary distribution functions f_1 and f_2 on in-going characteristics. The parts of the electron phase space that are free to be chosen are identified by the accessibility of characteristics to the boundaries (see section 2.1). The construction of the electron problem is similar to the Vlasov-Poisson problem in which a standard method used to obtain a solution is to fix the boundary distribution functions f and solve for the potential subject to the quasi-neutrality constraint. In our Vlasov problem a functional form of f at the boundaries is adopted on the basis of observations (see discussion in section 2.2). Specifying the cross-shock potential $\Delta\Phi^{\mathrm{HT}}$ and magnetic field jump, the shape parameters η, ν, ϕ, ψ, and A that define the boundary f are iteratively solved (step 3 in Figure 1) subject to quasi-neutrality (e.g., the downstream target density provided from the solution to the RH relations) and posed conditions on the upstream moments of f_1 (see section 2.4 for details). Once the shape parameters are determined, the downstream electron pressure can be calculated by quadrature (step 4). By subtracting the more tractable electron pressure P_{e2}^{mod} determined from f_2, the downstream ion pressure P_{i2}^{mod} and hence the downstream ion temperature can be obtained from the Rankine-Hugoniot predicted downstream pressure P_2^{RH} given by the following expression [*Whang*, 1987]:

$$P_2^{\mathrm{RH}} = P_1 - \rho_m U_n \Delta U_n - \Delta B^2/8\pi. \qquad (1)$$

In (1), $\rho_m = (m_p + m_e)N$ represents the plasma mass density. The Δ is used to denote the change of a physical quantity across the shock (e.g., $\Delta X \equiv X_2 - X_1$, where X_1 and X_2 are the upstream and downstream values of a physical quantity X). Observed shock quantities are used to set the values of the model inputs N_1, U_{n1}, $P_1 = P_{i1} + P_{e1}$, B_1, θ_{Bn1}, and $\Delta\Phi^{\mathrm{HT}}$. The resulting predictions of the theory are now determined and will be compared to observed downstream electron and ion temperatures.

2.1. Electron Vlasov Problem

The electron problem is based on the steady state Vlasov equation in the adiabatic approximation. In practice, solving self-consistently two steady state Vlasov equations (one for the electrons and one for the ions) and Maxwell's equations for the shock electromagnetic fields is a formidable task [*Morawetz*, 1961, 1962] because physical processes that determine the shock properties, such as the density variation, occur over a wide range of length and time scales. A useful approach is to solve the steady state Vlasov equation for the electrons in prescribed DC electric and magnetic fields given by

$$\mathbf{v} \cdot \frac{\partial \langle f \rangle}{\partial \mathbf{x}} + \frac{q}{m}\left[\langle \mathbf{E} \rangle + \frac{\mathbf{v} \times \langle \mathbf{B} \rangle}{c}\right] \cdot \frac{\partial \langle f \rangle}{\partial \mathbf{v}} = 0, \qquad (2)$$

where the explicit time variation of the background distribution is assumed to vanish (e.g., $\partial\langle f \rangle/\partial t = 0$) in the shock stationary frame. In (2), $\langle f \rangle$, $\langle \mathbf{E} \rangle$, and $\langle \mathbf{B} \rangle$ represent the average (or slowly varying) one-particle electron distribution function, electric field vector, and magnetic field vector, respectively. Thus, given $\langle \mathbf{E} \rangle$ and

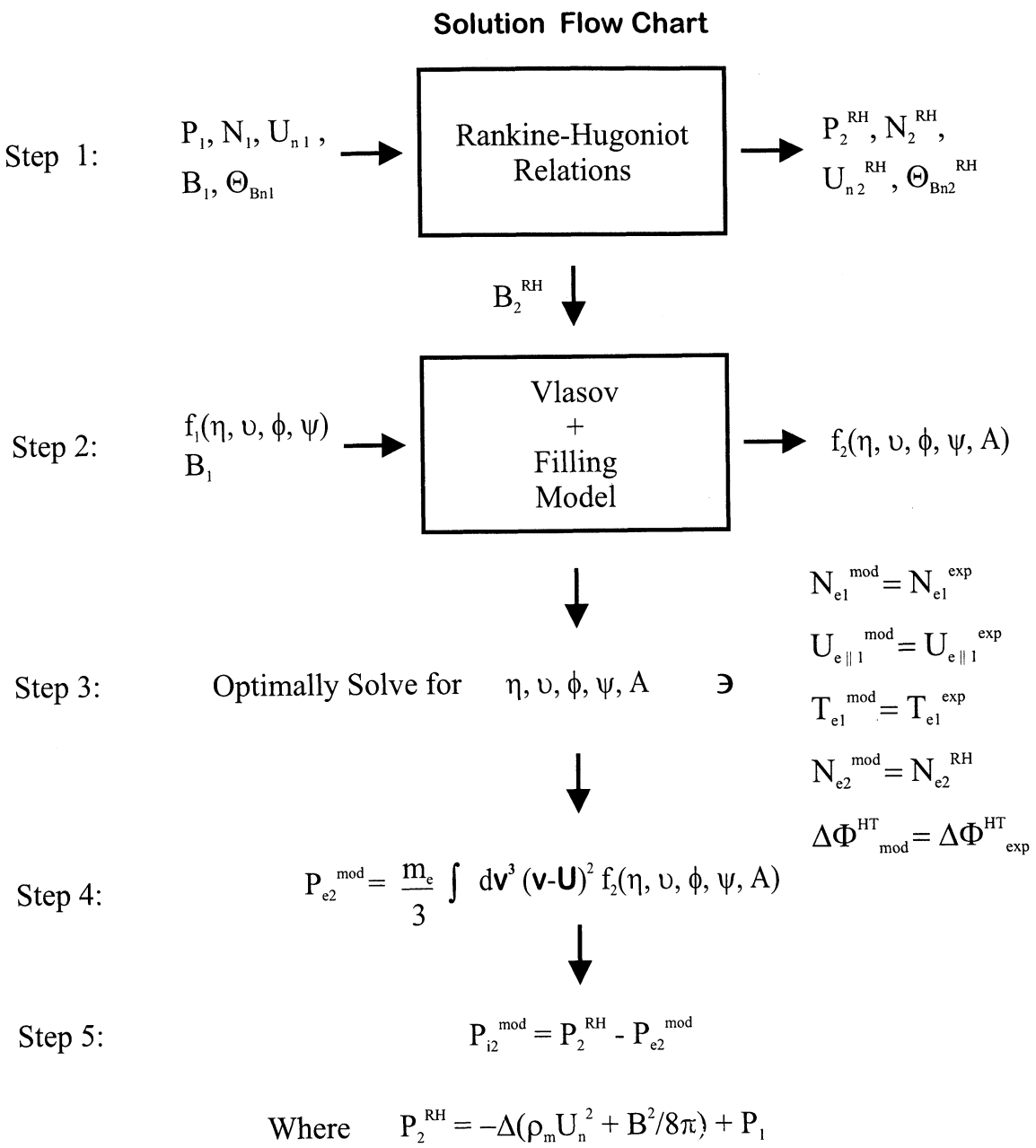

Figure 1. Flow diagram of model solution scheme.

$\langle \mathbf{B} \rangle$ the Vlasov equation is a linear first-order homogeneous partial differential equation which can be solved by the method of characteristics. In the remainder of the paper we adopt the more streamlined notation f, $\mathbf{E}$, and $\mathbf{B}$ when referring to the average macroscopic quantities.

We work in the HTF in solving the electron Vlasov problem because it is the simplest frame for describing electron kinematics. The characteristic curves along which f is a constant are defined by the electron orbits. However, not all of the electron orbits can access all phase space boundaries that define the shock system. In general, the determination of particle accessibility across time stationary, spatially varying electric and magnetic fields involves integration of particle orbits, unless there are enough constants of the motion to reduce the number of degrees of freedom in the system. In our model problem we take advantage of the conservation of electron energy and magnetic moment constraints specialized to HTF given by

$$E = \frac{1}{2} m_e \left[v_\perp^2(x) + v_{||}^2(x) \right] - e\Phi^{HT}(x) = \text{const}, \quad (3)$$

$$\mu = \frac{\frac{1}{2} m_e v_\perp^2(x)}{B(x)} = \text{const}, \quad (4)$$

where $v_\perp(x)$ and $v_{||}(x)$ are the local components of the HTF velocity of the electrons perpendicular and paral-

lel to the magnetic field, respectively. The generic accessibility of electron orbits to the boundaries defining the shock system allows us to determine electron phase space regions requiring a boundary condition specification. Under the assumption that the shock magnetic field is monotonic and that $\Phi^{\rm HT}(x)$ is linearly related to $B(x)$ [*Hull et al.*, 2000], downstream accessibility of upstream electron orbits is determined by the condition that $v_{2||} \geq 0$. Satisfying this condition, the downstream velocity components $(v_{2||}, v_{2\perp})$ are related to the upstream components $(v_{1||}, v_{1\perp})$ as follows:

$$ {v_{2||}}^2 = {v_{1||}}^2 + \left(1 - \frac{B_2}{B_1}\right){v_{1\perp}}^2 + \frac{2e}{m_e}\Delta\Phi^{\rm HT}, \quad (5) $$

$$ {v_{2\perp}}^2 = \left(\frac{B_2}{B_1}\right){v_{1\perp}}^2. \quad (6) $$

We will use observations to set the values for $\Delta\Phi^{\rm HT}$ and B_1 in order to test the predictions of the model with empirical estimates. The variable B_2 is determined from the RH jump relations given a few upstream constraints. The region of downstream electron velocity space within ultimately to the solar wind at the other connection point, the solar wind distribution should be a reasonable lowest-order estimate of this region of phase space, provided that the potential and the magnetic intensity at the two magnetically connected points do not differ substantially. Observational support for this approximation is provided by *Fitzenreiter et al.* [1990]. Contours of constant f_1 are indicated in Figure 2a, illustrating the mirroring signatures embedded in the model distribution. In the model distribution function, canonical values of .06 and 6.0 will be assumed for δ and γ, typical of the interplanetary medium at 1 AU. Furthermore, we assume that there is no slippage between the core and halo populations of the electron distribution function. In general, the core and halo populations have slightly different bulk speeds; however, this difference is typically much smaller than the parallel electron thermal speed. Therefore, in lowest order, we assume $\psi = \psi_c = \psi_h$ in (8) and (9) in order to simplify the problem and make it a more tractable one. Typically, the upstream electron distributions in the vicinity of the Earth's bow shock are slightly anisotropic with $T_{e||}/T_{e\perp} \sim 1.2$. Thus we assume $\omega = \omega_{||} = \omega_\perp$ in (8) and (9). However, even with this assumption, the upstream electron pressure is not guaranteed to be isotropic. With its in-going parts, f_1 has modest anisotropy and heat flux built into it. The upstream heat flux and thermal anisotropy could be constrained further, however, at the expense of adding more free parameters. A significant portion of the downstream distribution function f_2 is determined by f_1 via the V-L mapping. The downstream image of f_1 accessible to the downstream side of the shock (regions I′ and IV') is displayed in Figure 2b. Note that the region near the peak of f_1 gets energized and deformed forming a pillow in front of the elliptical separatrix (dashed curve) providing a natural explanation for the formation of electron beams found in the shock transition region and immediately behind the Earth's bow shock [*Feldman et al.*, 1983b]. The elliptical separatrix in Figure 2b distinguishes magnetosheath electron orbits that can access the upstream side of the shock (regions I′ and IV') from those magnetosheath electron orbits that can not (regions V and VI) because they get reflected by the electrostatic potential. The in-going distribution function in region V and its reflected counterpart in region VI need to have a nonvanishing assignment in order for a solution consistent with the RH expectation of the density ratio to be possible (see section 2.4). Motivated by observation of flat-topped electron distribution functions in the magnetosheath, we assign the distribution the ellipsoid defined by

$$ {v_{2||}}^2 + \left(1 - \frac{B_1}{B_2}\right){v_{2\perp}}^2 < \frac{2e}{m_e}\Delta\Phi^{\rm HT} \quad (7) $$

has no characteristics that connect to the upstream spatial boundary under the empirically motivated assumption $\Delta\Phi^{\rm HT} = \kappa\Delta B$. The electron distribution in this downstream velocity space region ${f_2}^{\rm ellipse}(\mathbf{v}_2)$ is a boundary condition that requires specification to be well posed. We demonstrate below that a nonzero ${f_2}^{\rm ellipse}(\mathbf{v}_2)$ specification is required in order to obtain a solution to the electron problem that is consistent with the RH compression (e.g., quasi-neutrality), a stronger condition than that the problem is well posed. The boundary conditions once appropriately specified provide a unique solution to the Vlasov equation via characteristics throughout the shock layer proper.

2.2. Model Electron Distribution Function

It is well known that any function of the constants of the motion is a solution to the Vlasov equation. This seems to suggest that the choice of the distribution function at the boundaries is somewhat arbitrary. However, we seek solutions of the time-independent Vlasov equation that are consistent with the RH downstream density that removes some of the freedom of an otherwise unconstrained Vlasov boundary value problem. A unique solution is possible with careful selection of the boundary conditions that further define the system under consideration. Because we wish to compare the results of the model to actual shock events, it is reasonable to use observations of electron distribution functions as a guide to select the functional form of the electron distribution function at the upstream and downstream spatial boundaries.

The shock layer with its electric and magnetic field gradients modifies the unperturbed solar wind distribution function by reflecting electrons back into the upstream medium, the reflected population showing up as a mirrored finite pitch angle high-energy tail in the upstream electron velocity distribution function [e.g.,

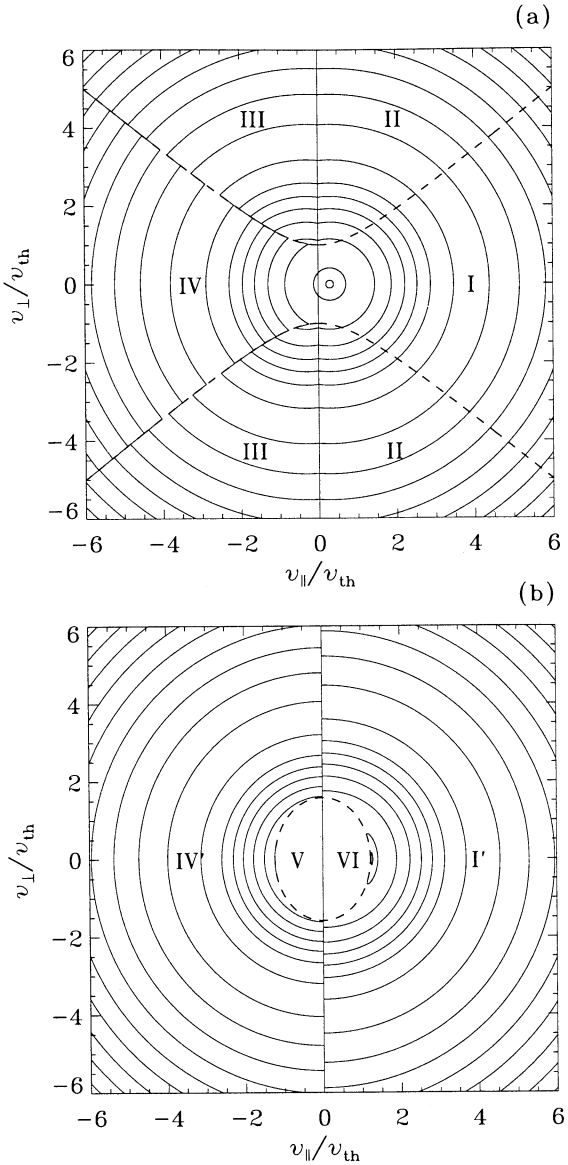

Figure 2. (a) Model upstream electron distribution function with modified loss cone separatrix indicated by dashed lines. Region I represents solar wind particles that have access to the downstream side of the shock, regions II and III represent the mirrored population, and region IV represents particles from the downstream side of the shock that leak into the upstream side of the shock. (b) Downstream model electron distribution function. Region V represents the ellipsoidal region which has no characteristics that connect to the upstream side. Regions I′ and IV′ represent the downstream image of regions I and IV, respectively.

Feldman et al., 1975; *Fitzenreiter*, 1995; *Klimas*, 1985, and references therein]. These nonlocal signatures of the approaching shock layer in the observed upstream electron distributions are naturally included in f_1 by using energy and magnetic moment conservation laws to construct a consistent model upstream electron velocity distribution function [*Hull et al.*, 1998]. The electron energy and magnetic moment constraints conspire to divide the upstream phase space into four distinct regions based on the source of the electrons and whether or not they have access to the other side of the shock [*Hull et al.*, 1998]. Figure 2a illustrates a generic modified loss cone separatrix (dashed lines) and the distinct regions anticipated on the upstream side of the shock. Region I represents solar wind electrons that can traverse the shock, while region II are solar wind electrons that cannot because they get mirrored from the shock. Region III represents the back-streaming electrons that have been previously reflected by the shock fields. Region IV represents magnetosheath electrons that can leak back into the upstream side of the shock along field lines. Because we desire a time stationary solution, regions that are dynamically connected must have boundary values that are consistent with Liouville's theorem.

An appropriate mirror-modified upstream distribution function must reflect the boundary conditions of the system that connect to each of the four distinct regions. We may thus consistently adopt the following functional form for f_1 [*Hull et al.*, 1998]:

$$f_1(\mathbf{v}_1) \equiv \begin{cases} f_{\rm ch}(v_{1||}, v_{1\perp}) & \text{Region I} \\ f_{\rm ch}(v_{1||}, v_{1\perp}) & \text{Region II} \\ f_{\rm ch}(-v_{1||}, v_{1\perp}) & \text{Region III} \\ f_{\rm ch}(v_{1||}, v_{1\perp}) & \text{Region IV,} \end{cases} \tag{8}$$

where the empirically motivated solar wind distribution used to construct $f_1(\mathbf{v}_1)$ is the core-halo model given by [*Feldman et al.*, 1975]

$$f_{\rm ch}(\mathbf{v}_1) = \frac{\eta(1-\delta)}{(\sqrt{\pi})^3\omega_{||}\omega_\perp^2}\exp\left(-\frac{(v_{1||}-\psi_{\rm c})^2}{\omega_{||}^2} - \frac{v_{1\perp}^2}{\omega_\perp^2}\right) + \frac{\eta\delta}{(\gamma\sqrt{\pi})^3\omega_{||}\omega_\perp^2}\exp\left(-\frac{(v_{1||}-\psi_{\rm h})^2}{\gamma^2\omega_{||}^2} - \frac{v_{1\perp}^2}{\gamma^2\omega_\perp^2}\right). \tag{9}$$

In (9), δ controls (but is not) the halo density fraction, and $\gamma^2 = T_{\rm h}/T_{\rm c}$ controls (but is not) the halo-core temperature ratio. The shape parameters η, $\omega_{||}$, $\omega_\perp$, $\psi_{\rm c}$, and $\psi_{\rm h}$ determine (but are not) the total density, core parallel thermal speed, core perpendicular thermal speed, and HTF parallel bulk speeds of the core and halo populations of $f_{\rm ch}$, respectively. The distribution in region IV is the upstream image of the in-going downstream magnetosheath electrons that traverse the shock layer from the sheath to solar wind side. In our model problem it is a boundary condition that is free to be chosen. Following *Fitzenreiter et al.* [1990], we set $f_1(v_{1||}, v_{1\perp}) = f_{\rm ch}(v_{1||}, v_{1\perp})$ in region IV. As discussed by *Fitzenreiter et al.* [1990], such a specification is not as arbitrary as it may seem. The magnetic field lines sufficiently close to the point of tangency will intersect the curved bow shock at two locations. Since the distribution in region IV is connected to the sheath and function in this ellipsoid region $f_2^{\rm ellipse}(\mathbf{v}_2)$ by using a mirror symmetric flat distribution model given by

$$f_2^{\text{ellipse}}(\mathbf{v}_2) = A f^{\text{sep}}(v_{2\perp} = 0), \quad (10)$$

where A, one of the shape parameters to be determined by the model, represents the level to which the ellipsoid is filled. The distribution function at the ellipsoidal separatrix boundary $f_2^{\text{sep}}(v_{2\perp})$ is given by

$$f_2^{\text{sep}}(v_{2\perp}) = \frac{\eta(1-\delta)}{\pi^{3/2}\omega^3} \exp\left[-\left(\frac{\psi}{\omega}\right)^2 - \left(\frac{\beta\psi}{\alpha\omega}\right)^2 {v_{2\perp}}^2\right] + \frac{\eta\delta}{\pi^{3/2}\gamma^3\omega^3} \exp\left[-\left(\frac{\psi}{\gamma\omega}\right)^2 - \left(\frac{\beta\psi}{\alpha\gamma\omega}\right)^2 {v_{2\perp}}^2\right], \quad (11)$$

where $\alpha^2 = (B_2 - B_1)/B_1$ and $\beta^2 = (B_2 - B_1)/B_2$.

2.3. Assumptions

In this paper we will be working in the HTF because in HTF the electrons are coupled to the ions only through the electrostatic potential. Consequently, we can circumvent the complex behavior of the ions and solve a more tractable Vlasov electron fluid-MHD problem for the downstream temperature partition. The RH relations used in the model neglect the heat flux vector, assume isotropic pressure, and treat the plasma as an adiabatic gas on either side of the shock. Thus the standard [*Boyd and Sanderson*, 1969] isotropic one-fluid pressure is related to the total plasma mass density as $P = S_0\rho_m^{\gamma}$, where S_0 is the entropy stream tube constant that, in general, changes across the shock layer and $\gamma = 5/3$. The isotropic pressure assumption for the plasma as a whole need not imply that the pressure tensors for the electrons, $\mathbf{P}_e$, and for the ions, $\mathbf{P}_i$, are isotropic, nor that $P_2/P_1 = (N_2/N_1)^{5/3}$.

In addition to conservation of electron energy, the model uses the following simplifying assumptions. First, the electrons are assumed to remain magnetized everywhere throughout the shock layer. Second, the field-aligned flow approximation mentioned above is invoked. With these two assumptions the electron magnetic moment is conserved, and the electron bulk flow remains along the same magnetic flux tube of force as the electrons traverse the shock in HTF. Third, the shock in the model is assumed to be a time stationary, planar layer. Fourth, the shock is assumed to have a monotonically increasing magnetic field profile. The fourth assumption more accurately describes weak shocks which tend to have laminar magnetic field profiles. Strong shocks tend to have nonmonotonic magnetic field profiles with a pedestal, overshoot, and undershoot region. Nonmonotonicity impacts electron accessibility, the details of which have been summarized in other studies [e.g., *Hull*, 1998; *Hull et al.*, 1997; Hull et al., Electron heating and phase space signatures at supercritical, fast mode shocks, submitted to *Journal of Geophysical Research*, 2000]. The model can be generalized to incorporate these nonmonotonic features to more accurately determine electron temperature changes at supercritical shocks.

In solving the Vlasov electron problem via the method of characteristics, the regions of downstream electron velocity space that can not access the upstream shock boundary is a boundary condition that is free to be specified (see section 2.1). Motivated by the pervasive flat-topped electron distribution functions observed behind strong fast mode shocks [*Montgomery et al.*, 1970; *Scudder et al.*, 1973, 1986a; *Feldman et al.*, 1983b], we make a fifth assumption that this region of downstream electron velocity space can be assigned with a flat-top distribution model, the level of which is proportional to the transmitted distribution function along the perimeter of the ellipsoidal separatrix boundary (see section 2.2). This assignment estimates contributions from magnetosheath electrons that have access to this ellipsoidal region of velocity space (but not the upstream boundary) and/or particles that get irreversibly scattered into this region via waves. A sixth assumption required for the V-L procedure [*Hull et al.*, 1998] is that there exists a functional relationship $\Delta\Phi^{\text{HT}} = \kappa\Delta B$, where ΔB is the magnetic field jump and κ is possibly a different constant for different shock layers. The theoretical model will use this relationship (which has empirical support [see *Hull et al.*, 2000]) to write the upstream distribution function as a function of the magnetic field jump and κ, among other variables.

2.4. Solution Scheme for the Shape Parameters

An important step in the determination of T_{e2} is to solve for the shape parameters η, ω, ψ, the assumed proportionality constant κ between $\Delta\Phi^{\text{HT}}$ and ΔB, and A, which parameterizes the distribution in the ellipsoid. To simplify the solution process, it is convenient to introduce the dimensionless parameters $\phi = v_\Phi/\omega = \sqrt{(2e\Delta\Phi^{\text{HT}}/m_e)}/\omega$, and $\nu = \psi/\omega$ and solve for the redefined set η, ψ, ϕ, ν, and A. A closed set of equations for η, ψ, ϕ, ν and A can be obtained with the help of the RH jump conditions; the V-L mapping procedure provides functional relations of the electron upstream density N_{e1}, upstream bulk speed $U_{e1||}$, upstream temperature T_{e1}, and the downstream density N_{e2} in terms of the HTF potential and the shape parameters. This is done by taking the appropriate velocity moments of f_1 and f_2 (see Appendix A for details on the upstream moments and Appendix B for the downstream moments):

$$N_{e1}(\eta,\phi,\nu) = \int d\mathbf{v}_1 f_1(\mathbf{v}_1), \quad (12)$$

$$U_{e1||}(\psi,\phi,\nu) = \frac{1}{N_{e1}} \int d\mathbf{v}_1 v_{1||} f_1(\mathbf{v}_1), \quad (13)$$

$$T_{e1}(\psi,\phi,\nu) = \frac{m_e}{3N_{e1}} \left\{ \int d\mathbf{v}_1 (v_{1||} - U_{e1||})^2 f_1(\mathbf{v}_1) + \int d\mathbf{v}_1 {v_{1\perp}}^2 f_1(\mathbf{v}_1) \right\}, \quad (14)$$

$$N_{e2}(\eta,\phi,\nu) = \int d\mathbf{v}_2 f_2(\mathbf{v}_2). \quad (15)$$

With the assumption that $\psi = \psi_c = \psi_h$, (13) is a separable function of ψ, ϕ, and μ (e.g., $U_{e1||}(\psi, \phi, \nu) = \psi v(\phi, \nu)$) and can be inverted to yield ψ as a function of ϕ and ν given the upstream electron bulk speed (see equation (A6)). The variables ϕ and ν can be determined for fixed A by zeroing the following composite function involving the upstream temperature $T_{e1}[\psi(\phi, \mu), \phi, \nu]$ and the compression ratio $\rho(\phi, \nu) = N_{e2}/N_{e1}$:

$$\mathcal{F}(\phi, \nu) = \mathcal{F}_T(\phi, \nu) + \mathcal{F}_\rho(\phi, \nu) = 0, \tag{16}$$

where

$$\mathcal{F}_T(\phi, \nu) = \frac{\left(T_{e1}|_{\rm BC} - T_{e1}[\psi(\phi, \nu), \phi, \nu]\right)^2}{T_{e1}^2|_{\rm BC}}, \tag{17}$$

$$\mathcal{F}_\rho(\phi, \nu) = \frac{\left[\rho|_{\rm RH} - \rho(\phi, \nu)\right]^2}{\rho^2|_{\rm RH}}. \tag{18}$$

The first term in (16) is a constraint imposed on ϕ and ν by the upstream electron temperature boundary condition $T_{e1}|_{\rm BC}$. The second contribution to (16) is a constraint on the electron density ratio $\rho(\phi, \nu) = N_{e2}/N_{e1}$. In general, the density ratio is a function of A through N_{e2}; however, in solving for ψ, ϕ, and ν we fix A to be a nonzero value and then adjust its value until $\Delta\Phi^{\rm HT}_{\rm mod}$ converges to $\Delta\Phi^{\rm HT}_{\rm exp}$. Any solution to the Vlasov equation will be consistent with the conservation of number flux across a time stationary shock, but it is not guaranteed that N_{e2} will match the RH expectation under quasi-neutrality and zero current assumed on both the upstream and downstream asymptotic states. Consistency with RH is achieved by requiring $\rho(\phi, \nu) = \rho_{\rm RH}$, where $\rho_{\rm RH}$ is the RH predicted electron density ratio. The parameter ψ can be determined from (13) and (A5) once the optimal values for ϕ and ν have been determined. The last parameter η is then determined from (12) and (A2). We demonstrate that a solution to (16) is not possible if we set $f_2{}^{\rm ellipse} = 0$; this is demonstrated graphically in the top panel of Figure 3, which shows that the zero-level curve of $\mathcal{F}_T$ (solid line) does not intersect the point where $\mathcal{F}_\rho = 0$ (under the assumption that $N_{e2}{}^{\rm ellipse} = 0$ in (12) and (B3)). However, a unique solution to (16) can be found by filling the ellipsoid to a level proportional to the average value of f_2 along the separatrix perimeter. The unique solution to (16) is indicated by the asterisk in the bottom panel of Figure 3 at the intersection of the zero-level curves of $\mathcal{F}_T$ (solid) and $\mathcal{F}_\rho$ (dashed). Figure 3 demonstrates the need to specify a nonvanishing $f_2{}^{\rm ellipse}$ for the problem to be consistent with the electrodynamics of quasi-neutrality, a stronger condition than that it is a "well-posed" Vlasov problem. Part of the f_2 is determined by employing Liouville's theorem to map the f_1 along characteristics to the downstream side. The $f_2{}^{\rm ellipse}$ cannot be arbitrarily defined and still satisfy the time-independent RH equations with a quasi-neutral fluid. The parameter A is determined by iteration subject to the constraint $\Delta\Phi^{\rm HT}_{\rm mod} = \Delta\Phi^{\rm HT}_{\rm exp}$.

3. Model Results on ΔT_e

The predictions of the model for $\Delta T_e{}^{\rm mod}$ are compared to experimental values for $\Delta T_e{}^{\rm exp}$ from an extensive electron moment and magnetic field data set of 129 Earth bow shock crossings observed by ISEE 1. The electron measurements, taken by the Vector Electron Spectrometer (VES) on board ISEE 1 [*Ogilvie et al.*, 1978], were corrected for the spacecraft floating potential and characterized by the best possible determination of the local shock geometry and shock velocity via an RH analysis [*Hull et al.*, 2000]. The shock data set encompasses a variety of shock conditions and includes some events with unusually large $\Delta T_e{}^{\rm exp}$ featured in earlier studies [*Thomsen et al.*, 1987; *Schwartz et al.*, 1988]. The results of the model for the electron temperature changes are summarized in Plate 1. Plates 1a–1c are comparisons of the predictions of the model (x axis) and the observed changes (y axis) in the parallel, perpendicular, and total electron temperature, respectively. These plots are color-coded to illustrate the dependence on the HTF upstream electron thermal Mach number $M_{\rm HTF1} = U_{n1}/(V_{\rm the1}\cos\theta_{Bn1})$, where U_{n1} and $V_{\rm the1}$ represent the upstream normal bulk flow and the electron thermal speed, respectively. Values of $M_{\rm HTF1} \gtrsim 1$ indicate where the field-aligned electron flow approximation [*Scudder*, 1987] is expected to break down because electron inertia is no longer negligible. In this regime, the typical electron has difficulty responding to magnetic field gradients and tends to slip magnetic field lines while traversing the shock layer. Such a regime requires a more complicated V-L mapping than that undertaken here.

Plates 1a–1c show that in addition to recovering the total temperature changes, the model also recovers the trends in the perpendicular and parallel degrees of freedom throughout the entire range of observations including the extreme values of ΔT_e ($\gtrsim 200$ eV). It is not clear why the Vlasov model should work in the regime where the field-aligned flow approximation breaks down. One possible explanation is that the slippage across magnetic field lines associated with large electron inertia is suppressed by the magnetic field's tight grip on the electron orbits implied by a lower β_e. The events characterized by large $M_{\rm HTF1}$ in this paper tend to have smaller β_e and vice versa [*Hull et al.*, 2000]. The limit of small β_e usually corresponds to the small gyroradius limit. In this regime, electrons only get energized by $\Delta\Phi^{\rm HT} \approx -\int dx E_{||}/(\hat{\mathbf{n}}\cdot\hat{\mathbf{b}})$ (where $E_{||}$ is the electric field component parallel to the magnetic field unit vector $\hat{\mathbf{b}}$) as the electrons follow a common path along magnetic field lines in traversing the shock maintaining constant μ [*Goodrich and Scudder*, 1984]. For the high β_e and high $M_{\rm HTF1}$, cross-field drifts such as grad B

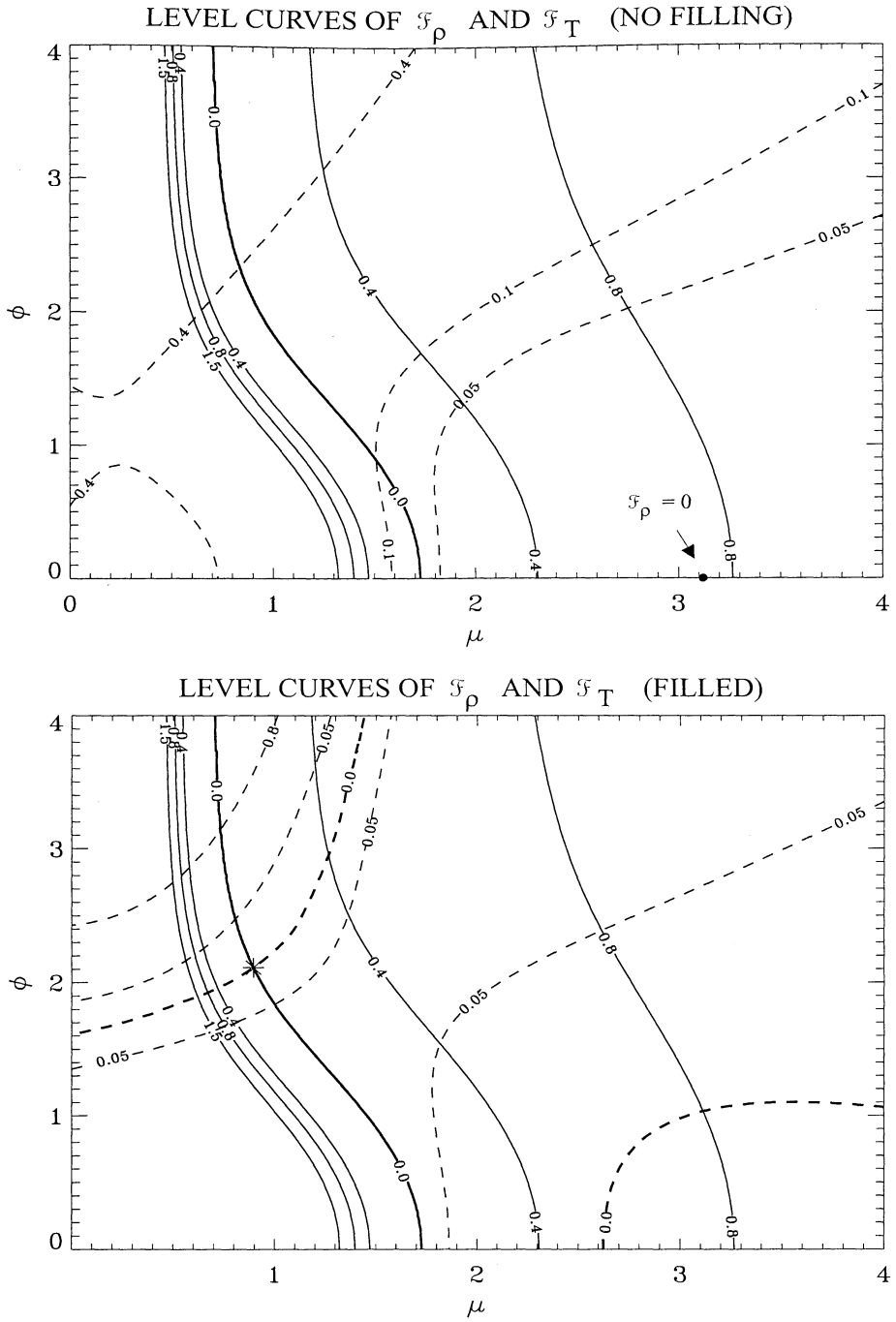

Figure 3. (top) graph showing that $\mathcal{F}(\phi, \nu)$ can not be zeroed when the ellipsoid is not filled. (bottom) graph showing that there exists ϕ and ν such that $\mathcal{F}(\phi, \nu) = 0$ when the ellipsoid is filled.

and curvature drifts become more important and impact electron energetics as the electrons are no longer field-aligned. The V-L mapping in this regime must conserve generalized momenta and need not be accomplished field line by field line as in our model. The cross-field drift V_d that the typical electron in this regime undergoes effectively enhances the accelerating normal electric field the electrons see in traversing the shock by $E_n^{\rm eff} \approx E_{||}/(\hat{\mathbf{n}} \cdot \hat{\mathbf{b}}) + V_d B_y$, similar to the way ion drifts along the shock surface in HTF enhance the decelerating normal electric field the typical ion sees in traversing layer.

The experimental study by *Hull et al.* [2000] found that ΔT_e is linearly related to $\Delta\Phi^{\rm HT}$ with a slope $\langle\alpha\rangle = 2.0 \pm 0.1$. *Hull et al.* [2000] suggested that this is indicative of a polytrope with an average effective poly-

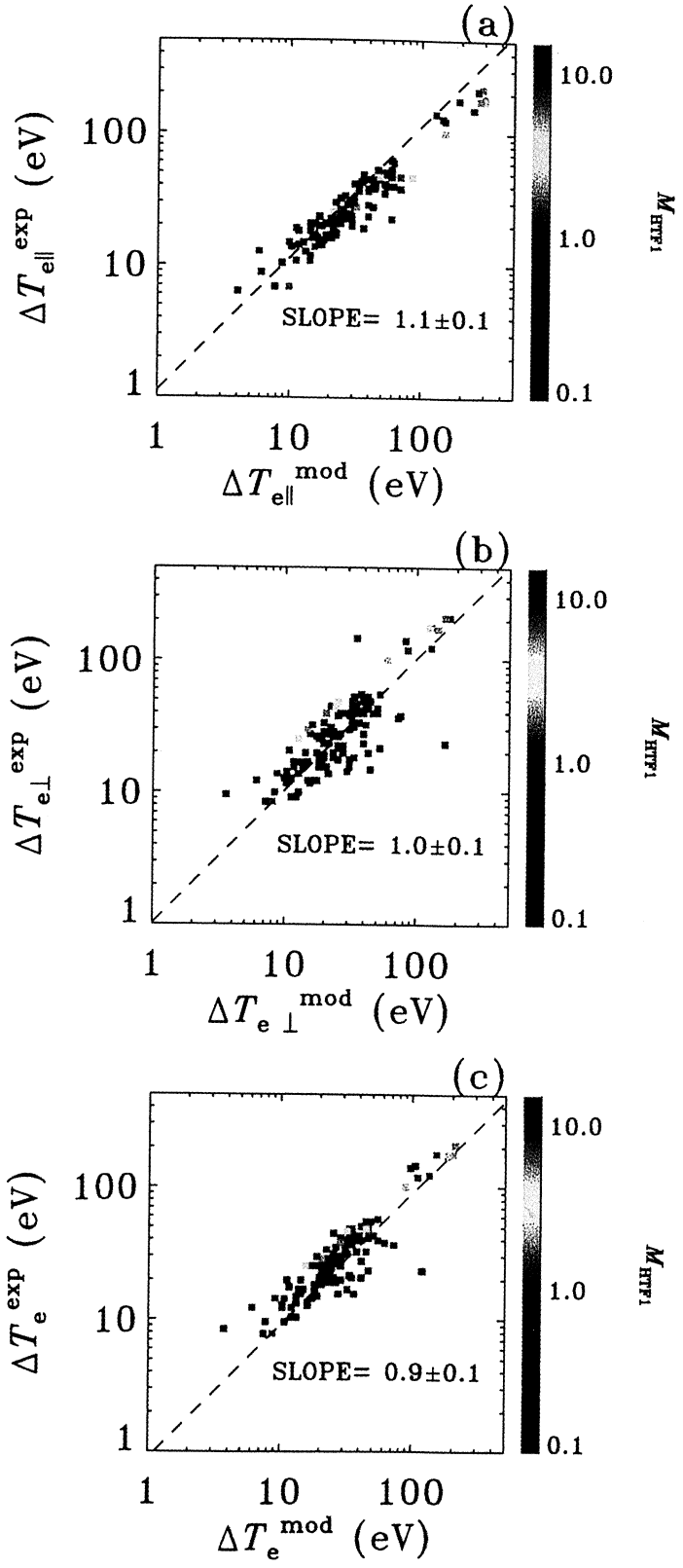

Plate 1. Comparisons between the predictions of the model and the observed changes in the (a) parallel, (b) perpendicular and (c) total electron temperatures across the database of shock events. The color indicates the M_{HTF1} dependence.

trope index $\langle\gamma_{\rm eff}\rangle = \langle\alpha\rangle/(\langle\alpha\rangle - 1) = 2.0 \pm 0.1$. *Hull et al.* [2000] further demonstrated that this is consistent with the most probable $\gamma_e = 2.4 \pm .8$ determined from fits to $N_e(t)$ and $T_e(t)$ [*Hull*, 1998]. Implicit in the model's recovery of the ΔT_e is the recovery of this linear relationship between ΔT_e and $\Delta\Phi^{\rm HT}$ (e.g., the recovery of the electron polytrope behavior). The model's recovery of the relation between ΔT_e and $\Delta\Phi^{\rm HT}$ is not circular, as might be suspected from the $\Delta\Phi^{\rm HT}$ constraint imposed on the model. The expressions (A9), (A10), (B11), and (B13) used to derive ΔT_e are nonlinear functions of $\Delta\Phi^{\rm HT}$, suggesting that the recovery of the linear relationship between ΔT_e and $\Delta\Phi^{\rm HT}$ is not guaranteed. Of particular note is the fact that the polytropic behavior is born out of the model which is based on a fully reversible description of electron behavior across the shock. A polytrope relation is a simplifying mathematical closure approximation that is not well understood. The model suggests that the underlying physics is adiabatic motion of electrons in the shock macroscopic electromagnetic fields; a consequence of the Vlasov connectivity seems to be this unsuspected local functional relationship between P_e and N_e.

4. Predicted Scaling of κ

For a number of shock crossings, depending on the electron β_e, the incremental changes in the magnetic field δB were found to be proportional to the incremental changes in the HTF potential $\delta\Phi^{\rm HT}$ with a proportionality constant κ assumed to be a fixed constant for a given shock crossing [*Hull et al.*, 2000]. Such a relationship has important implications on the dynamics of electrons across the shock and motivates the relationship $\Delta\Phi^{\rm HT} = \kappa\Delta B$ exploited by the model. The electron moment dependence on κ is implicit in the dimensionless potential $\phi = v_\Phi/\omega = \sqrt{(2e\kappa\Delta B/m_e)}/\omega$. An approximate expression for κ in terms of upstream conditions and shape parameters can be derived from (A5) by taking advantage of the fact that the halo density fraction, δ, is usually small and by solving for the dimensionless potential ϕ perturbatively. Under the assumption that δ is small, (A5) reduces to

$$U_{e1||} \approx \psi\left[\frac{1-\beta^3\exp(-\xi_c^2)}{1+\beta\exp(-\xi_c^2)\ \mathrm{erf}(\beta\nu)}\right], \qquad (19)$$

where $\beta^2 = (B_2 - B_1)/B_2$ and $\xi_c^2 = \phi^2/\alpha^2 + \lambda^2\nu^2$ with $\alpha^2 = (B_2 - B_1)/B_1$ and $\lambda^2 = 1 - \beta^2$, respectively. Rearranging (19) and solving for ϕ yields the following expression for the lowest-order estimate of κ^0:

$$\kappa^0 \approx \frac{m_e\omega^2}{2eB_1}\ln\sigma, \qquad (20)$$

where

$$\sigma = \left(\frac{U_{e1||}\beta\ \mathrm{erf}(\beta\nu) + \psi\beta^3}{\psi - U_{e1||}}\right)e^{-\lambda^2\nu^2}. \qquad (21)$$

Equation (20) predicts that κ should scale as the magnetic moment per unit charge of a typical thermal electron. The interpretation of the scaling in (20) is that a significant fraction of the upstream electron distribution must make it through the shock in order to satisfy the plasma's desire to be quasi-neutral [*Hull et al.*, 2000]. The $\ln\sigma$ factor, although a fixed constant for a given shock crossing, is not guaranteed to be a global constant and should vary depending on shock conditions.

To test the predicted scaling, we computed κ from $\Delta\Phi^{\rm HT}$ and ΔB for the 129 shock events used in this paper. The ratio $r_{\rm scale} = \kappa/(kT_{e\perp 1}/eB_1)$ is summarized in the histogram illustrated in Figure 4. The most probable ratio $\tilde{r}_{\rm scale}$ suggests that electrons with perpendicular energies below roughly 3 times the perpendicular thermal energy within the modified loss cone make it through the shock layer. This represents $[1-\exp(-3)] \sim .95$ of the thermal electrons. The $r_{\rm scale}$ in Figure 4 are not Gaussian distributed, having a tail toward higher values of $r_{\rm scale}$. These events are characterized by higher values of $\beta_e \gtrsim 1$. The measurements that determine $r_{\rm scale}$ in these shock events are highly aliased and should be viewed with caution. The spread in the distribution probably reflects κ's dependence on other characteristic shock parameters such as $M_{\rm HTF1}$, $\Delta(m_pU_n^2/2)$, and θ_{Bn1}. The relationship between κ and other characteristic shock parameters will be explored in future work.

5. Model Results on T_i

The model prediction of the downstream ion temperature $T_{i2}^{\rm mod}$ is determined by subtracting the model determination of the electron pressure from the RH expectation of the total pressure change $\Delta P^{\rm RH}$ given by (1). For comparisons with the model, we have used a previously cataloged ion data set [*Thomsen et al.*, 1987;

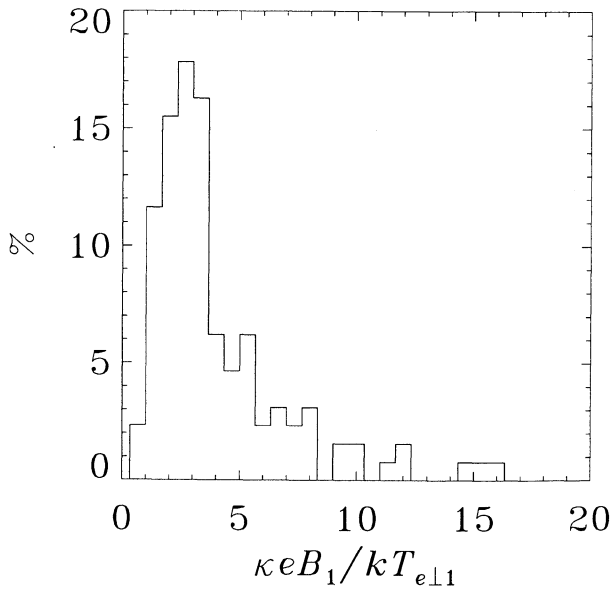

Figure 4. Histogram of the ratio $\kappa/(kT_{e\perp 1}/B_1)$.

Schwartz et al., 1988] measured by the Solar Wind Experiment (SWE) on the solar wind side and by the Fast Plasma Experiment (FPE) on the downstream side of the shock [see *Bame et al.*, 1978, for instrument details]. Ion temperatures were available for only 38 of the shock crossings used in this study. Averages of the maximum and minimum values at the shock asymptotes were used to estimate the upstream and downstream ion temperatures. The reported total ion temperature was approximated by the FPE team as $T_i = (T_{i||} + T_{i\perp})/2$; this approximation has the effect of systematically underestimating/overestimating the temperature computed via trace$(\mathbf{P_i})/(3N_i)$ ($\mathbf{P_i}$ and N_i are the ion pressure tensor and ion density, respectively) when $T_{i||}$ is less/greater than $T_{i\perp}$. This effect is relatively small in the limit of small anisotropy, which tends to be the case. The shock geometry was determined via an RH analysis using electron data measured by the VES instrument on ISEE 1. We did not have ion flow vectors, thus electron flows and densities in addition to magnetic field data were used to compute ΔP^{RH}.

Figure 5a compares ΔP^{RH} to the observed total pressure change ΔP^{exp}. In Figures 5b and 5c the resulting model predicted ion pressure change $\Delta P_i{}^{\mathrm{mod}}$ and downstream ion temperature $T_{i2}{}^{\mathrm{mod}}$ are compared to the observed ion pressure change $\Delta P_i{}^{\mathrm{exp}}$ and observed downstream ion temperature $T_{i2}{}^{\mathrm{exp}}$, respectively. The vertical error bars indicated in Figures 5a-c provide a lower bound error estimate, representing the propagated uncertainty associated with the average asymptotic electron moment and magnetic field quantities used to compute ΔP^{RH}, $\Delta P_i{}^{\mathrm{mod}}$, and $T_{i2}{}^{\mathrm{mod}}$, respectively. The open circles represent shock crossings characterized by normal shock propagation speeds in the S/C frame of reference that are greater than 150 km s^{-1}, determined from the RH analysis using electron data. Because of the speed at which these shocks convect by the S/C, the asymptotic states of these atypical bow shock events are not accurately determined. The best fit slope indicated by the dashed lines in Figures 5a-c suggests that the model predictions ΔP^{RH}, $\Delta P_i{}^{\mathrm{mod}}$, and $T_{i2}{}^{\mathrm{mod}}$ are consistent with their observed counterparts over the range of shock conditions, though there is considerable scatter. The correlation coefficients for the comparisons in Figures 5a-c are 0.79, 0.69, and 0.62, respectively. Because the ram energy contribution to the change in pressure is weighted by the ion mass, small errors in the empirical estimates of the normal flow speed and density can result in large changes in energy available for heating and hence errors in the predicted ion temperature. As an illustration of the sensitivity to errors in the flow, a canonical normal electron bulk flow of 300 km s^{-1} with an error of 25 km s^{-1} gives rise to an error in the model downstream ion temperature $\delta(\Delta T_i) \approx 2m_p U_n \delta U_n = 2 \times 10^6$ K comparable to many of the error bars in Figure 5c. A modest relative uncertainty in the density of $\delta N_1/N_1 = .2$ gives rise to similar errors in $T_{i2}{}^{\mathrm{mod}}$. In addition to this complication, the

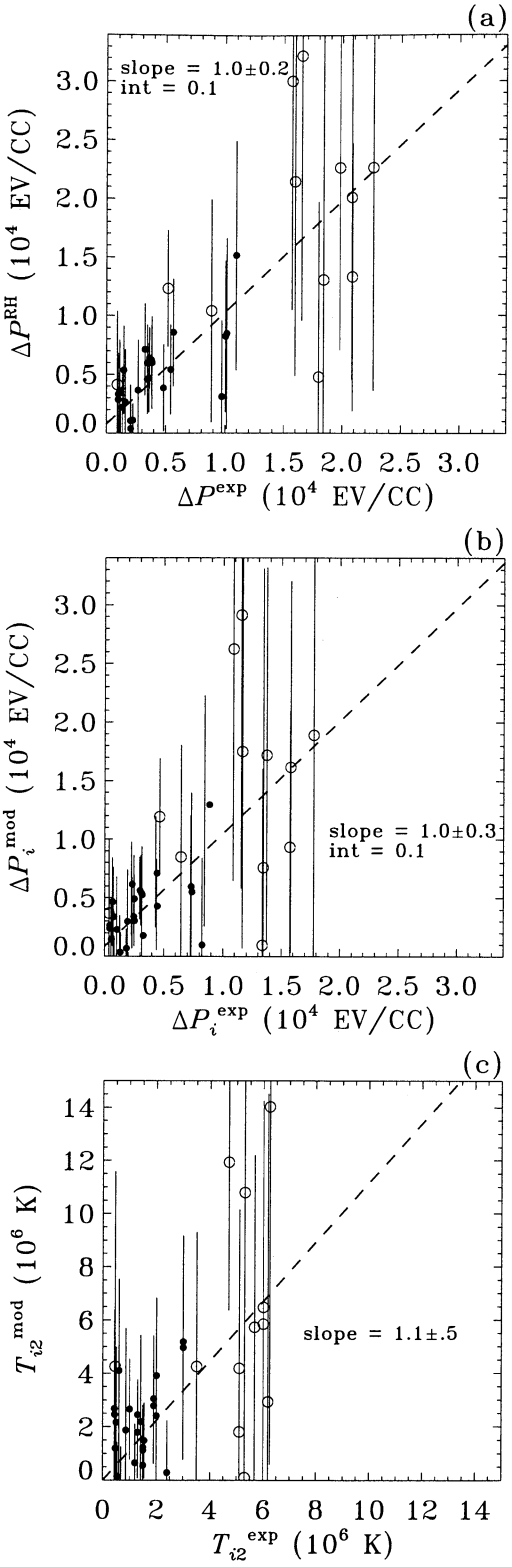

Figure 5. Comparisons of the model predictions for (a) the total pressure change ΔP^{RH}, (b) the ion pressure change $\Delta P_i{}^{\mathrm{mod}}$, and (c) the downstream ion temperature $T_{i2}{}^{\mathrm{mod}}$ with the observed total pressure change ΔP^{exp}, ion pressure change $\Delta P_i{}^{\mathrm{exp}}$ and downstream ion temperature, $T_{i2}{}^{\mathrm{exp}}$, respectively.

VES electron detector and the ion sensors were not intercalibrated. Systematic departures between these detectors can also impact the results. Despite these problems the model approximately recovers the observed total pressure change and hence the ion pressure change and downstream ion temperature for a variety of shock upstream conditions. It is our opinion that the propagated uncertainties associated with the electron bulk speed and density and the systematic uncertainties between the electron and ion detectors do not detract from the attractive explanation for the partition of temperature advanced by the Vlasov mapping of this paper.

6. One-Sided Predictive Model

One of the goals of this paper is to develop a one-sided predictive model for the partition of temperature for the electrons and ions as they traverse the shock layer. The model developed in sections 2.1–2.4 relied on the measured two-point $\Delta\Phi^{HT}$ as a constraint in order to recover the electron temperature changes for a variety of shock conditions. The $\Delta\Phi^{HT}$ was needed to constrain the electron distribution function ${f_2}^{ellipse}$ at the downstream boundary inaccessible to the upstream side. Without this constraint the assignment of ${f_2}^{ellipse}$ would be arbitrary. The development of a one-sided version of the model requires a recipe for specifying the downstream boundary ${f_2}^{ellipse}$ essential for a well-posed problem in terms of upstream conditions, and hence $\Delta\Phi^{HT}$ can be determined so that quasi-neutrality is satisfied. The virtue of using $\Delta\Phi^{HT}$ to constrain ${f_2}^{ellipse}$ is that it allows for the possibility of "learning" how to specify ${f_2}^{ellipse}$. The existence of such a recipe is suggested in Figure 6, which compares the filling level A of ${f_2}^{ellipse}$ with M_{HTF}. A polynomial fit to A and M_{HTF} in semilog space yields

$$A = \exp(-2.3 + 1.2M_{HTF} + 0.13{M_{HTF}}^2). \quad (22)$$

The expression (22) suggests that the two-sided property of the V-L problem could be broken by such an empirical basis.

With the adopted filling recipe (expression (22)) the V-L-based electron problem is carried out in a manner similar to the two-point problem discussed above, except now the downstream level is determined by (22) and $\Delta\Phi^{HT}$ is a fit parameter, determined so that the upstream boundary conditions and the RH expectation on the downstream density are satisfied. The one-sided model predictions on the electron pressure change ${\Delta P_e}^{pred}$ are compared to the observed electron pressure change ${\Delta P_e}^{exp}$ in Figure 7a. Figure 7a shows that the ${\Delta P_e}^{pred}$ is in good agreement with the ${\Delta P_e}^{exp}$ throughout most of the range of observations. The correlation coefficient is 0.7, and the best fit slope (dashed line) is .97±.10 in Figure 7a. Figure 7b compares the predicted temperature change ${\Delta T_e}^{pred}$ to the observed temperature change ${\Delta T_e}^{exp}$. The ${\Delta T_e}^{pred}$ values are in rough

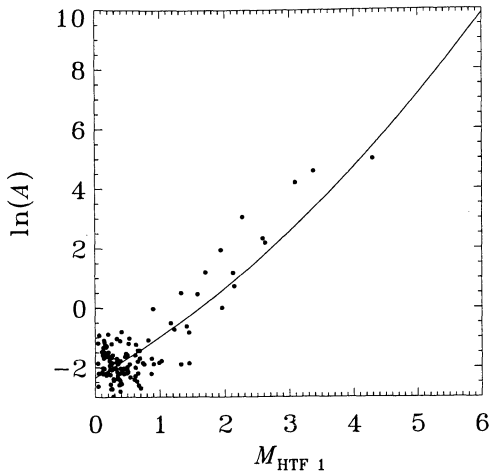

Figure 6. Comparisons of A with M_{HTF}.

agreement with the observations, although the model results are smeared out (correlation coefficient is .6) compared to the two-sided results illustrated in Plate 1c. The model's less accurate ${\Delta T_e}^{pred}$ determination reflects inaccuracies introduced by specifying ${f_2}^{ellipse}$ using (22). The moment temperature is of the following form:

$$kT_e = \frac{P_e}{N_e} \equiv \frac{m_e}{3}\frac{\int_0^\infty f(\mathbf{v})v^4 dv \sin\theta d\theta d\phi}{\int_0^\infty f(\mathbf{v})v^2 dv \sin\theta d\theta d\phi}. \quad (23)$$

Because of the integrand's v^4 dependence, ${P_{e2}}^{pred}$ is relatively immune to inaccuracies in assigning the form of ${f_2}^{ellipse}$, with much of the contribution to the downstream pressure coming from regions outside the oval. The model downstream electron temperature ${T_{e2}}^{pred}$, however, is much more sensitive to inaccuracies in ${f_2}^{ellipse}$ because of the denominators v^2 dependence. While the model fit of (22) recovers the trends in ΔP_e, more accurate ΔT_e requires a more faithful reproduction of $\Delta\Phi^{HT}$. Note that the dispersion in Figure 7b at low ΔT_e is where errors of 100% in $\Delta\Phi^{HT}$ are common place when using (22) as an empirical basis to remove the inherent two-sidedness of the Vlasov equation. The one-sided model provides substantially more accurate predictions of the downstream electron pressure and temperature and hence downstream ion pressure and temperature from one-fluid conservation laws than do estimates provided under the equipartition assumption.

Under equipartition the electrons and ions are assumed to have equal pressure. The equipartition expectation on the electron pressure change $\Delta P_e^{eq} = \Delta P/2$ is computed from (1) using moment and field data. Figures 7c and 7d compare the equipartition expectation on ΔP_e^{eq} and electron temperature jump ΔT_e^{eq} to observations, respectively. Clearly, Figures 7c and 7d demonstrate that equipartition fails miserably, tending to overestimate the ΔP_e and hence ΔT_e over the broad range of shock conditions as indicated by the best fit

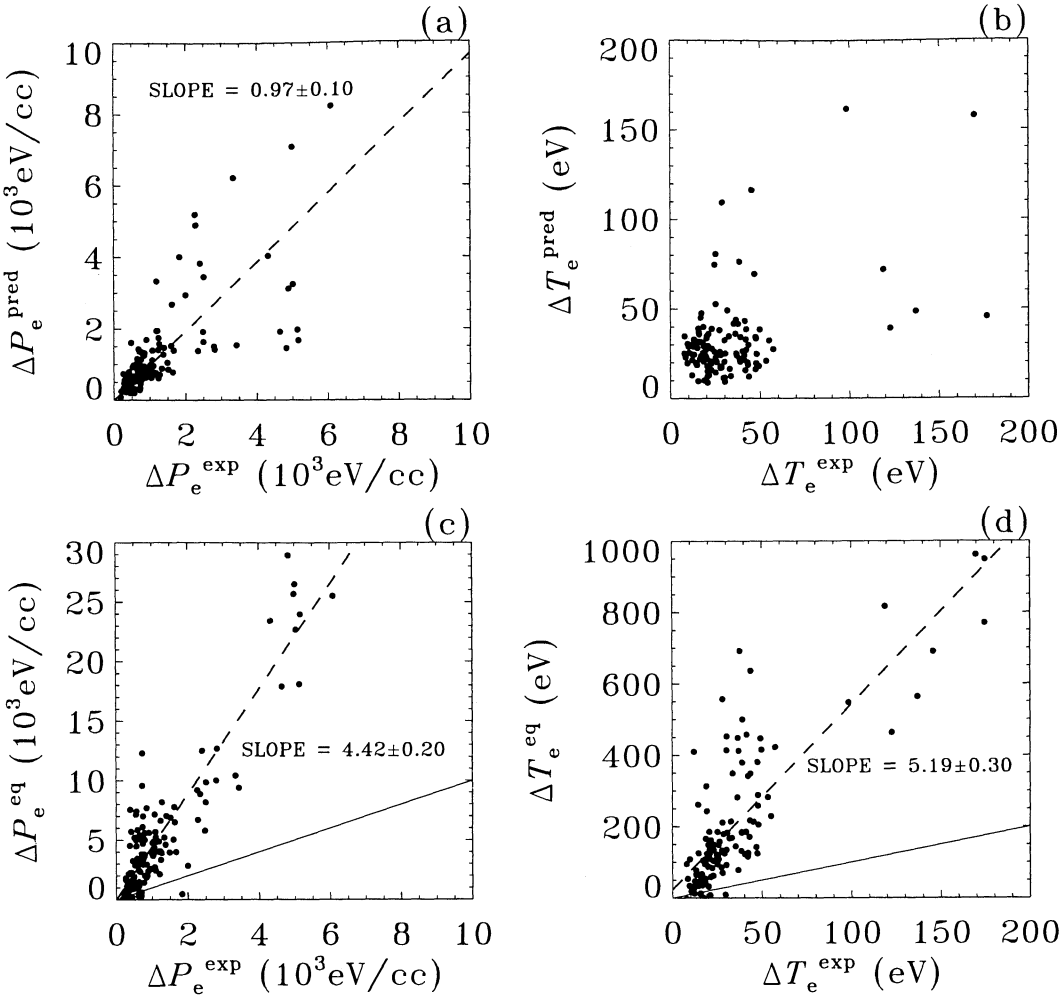

Figure 7. Comparisons of (a) the one-sided model predictions on the electron pressure change $\Delta P_e{}^{\rm pred}$ and (b) temperature jump $\Delta T_e{}^{\rm pred}$, with the observed pressure change $\Delta P_e{}^{\rm exp}$ and temperature change $\Delta T_e{}^{\rm exp}$, respectively, and comparisons of (c) the equipartition expectation on the electron pressure change $\Delta P_e{}^{\rm eq}$ and (d) temperature jump $\Delta T_e{}^{\rm eq}$, with $\Delta P_e{}^{\rm exp}$ and $\Delta T_e{}^{\rm exp}$, respectively.

slopes (dashed line) of $4.4 \pm .2$ and $5.2 \pm .3$ in Figures 7c and 7d, respectively. The solid lines in Figures 7c and 7d indicate unity slope. Overestimating ΔP_e implies that equipartition will underestimate the ion pressure change. For this reason, results of models which use the equipartition assumption must be viewed with caution.

7. Conclusions

The downstream partitioning of temperature between electrons and ions across collisionless shocks is viewed as the result of the different modes in which the electrons and ions interact coherently with the same shock layer: the ions are unmagnetized; the electrons are nearly fully magnetized. However, the differential response of the electrons and ions to the shock field structure makes solving the Vlasov-Maxwell problem an arduous task. To circumvent the difficulties associated with the numerically stiff Vlasov-Maxwell problem, we have developed an approximate multilevel model for the partition of temperature that incorporates the simple behavior of electrons across collisionless, fast mode shocks, and we compared the predictions of the model to a large database of Earth's bow shock crossings. For the first time the trends in the perpendicular and parallel electron temperature jumps and therefore ΔT_e for the "typical" as well as the "extremes" of the observations have been recovered. The trends in the ion pressure jump and hence the ion temperature jump determined by subtracting the model-predicted downstream electron pressure from the total downstream pressure predicted by RH are also recovered. By inference, the results of the model support the notion that in HTF the electrons are coupled to the ions only through $\Delta\Phi^{\rm HT}$ and that the

wave-particle coupling between electrons and ions can be neglected in lowest order.

Implicit in the model's recovery of ΔT_e is the recovery of the linear relationship ΔT_e and $\Delta\Phi^{\rm HT}$ [*Hull et al.*, 2000] which is a reflection of the average electron polytropic behavior through the shock layer. Recovery of the linear relationship between ΔT_e and $\Delta\Phi^{\rm HT}$ is quite remarkable and not obvious from (A8), (A10), (B10), and (B13), which are nonlinear functions of $\Delta\Phi^{\rm HT}$ that determine ΔT_e. The model suggests that the electron polytrope relation is the macroscopic restatement of the Lagrangian free-streaming motion of magnetized electrons through the shock macroscopic fields.

We determined theoretically that the empirically suggested κ parameter [*Hull et al.*, 2000], which relates the HTF potential increments to the magnetic field increments through the shock, scales in leading order with the average upstream electron magnetic moment. We demonstrated that this scaling was consistent with that inferred from observations. Viewed as an equation of state relating the microphysical properties of the plasma to the macrostate of the shock, the relation $\Delta\Phi^{\rm HT} = \kappa\Delta B$ summarizes the tension between the tendency of the magnetic field to repel electrons and the desire for the plasma to maintain quasi-neutrality with zero current along the shock normal. The lowest-order scaling of κ with respect to $kT_{e\perp 1}/B_1$ reflects the fact that a significant fraction of the electron population must traverse the shock layer to satisfy quasi-neutrality, since the supersonic ion's inertia virtually guarantees that most of the ions jump the layer.

Given what was learned from the two-sided model, a version of the model was developed to estimate the electron pressure change and hence the electron temperature change given only few upstream constraints. This one-sided version of the model roughly recovers the observed electron pressure and temperature change with much greater accuracy than do models which employ the equipartition assumption. The equipartition expectation was shown to overestimate the electron temperature change by a factor 4.4, which leads to underestimated downstream ion temperatures. More precise predictions from the one-sided model requires more precise recovery of $\Delta\Phi^{\rm HT}$.

Appendix A: Upstream Electron Moments

Velocity moments of f_1 and f_2 result in transcendental equations that can then be solved to yield the shape parameters of f_1 and f_2 so that the Rankine-Hugoniot relations and the conditions on the upstream moments of f_1 are satisfied. We give analytic expressions for the upstream moments in terms of the shape parameters of f_1 and f_2. Upstream electron moments involve integrals of the form

$$\int d^3\mathbf{v}_1 f_1(\mathbf{v}_1)\mathcal{H}(\mathbf{v}_1), \qquad \text{(A1)}$$

where $\mathcal{H}(\mathbf{v}_1)$ is a function of the upstream velocity.

A1. Upstream Electron Density

Setting $\mathcal{H}(\mathbf{v}_1) = 1$ in (A1) yields the upstream electron density:

$$N_{e1}(\eta,\phi,\nu) = \eta(1-\delta)\left[1+\beta e^{-\xi_c^2}\mathrm{erf}\left(\beta\nu\right)\right] + \eta\delta\left[1+\beta e^{-\xi_h^2}\mathrm{erf}\left(\frac{\beta\nu}{\gamma}\right)\right], \qquad \text{(A2)}$$

where

$$\xi_c^2 = \phi^2/\alpha^2 + \lambda^2\nu^2, \qquad \text{(A3)}$$

$$\xi_h^2 = \frac{\phi^2/\alpha^2 + \lambda^2\nu^2}{\gamma^2}, \qquad \text{(A4)}$$

with the following ancillary definitions: $\nu = \psi/\omega$; $\phi = v_\Phi/\omega$; $\alpha^2 = (B_2-B_1)/B_1$; $\beta^2 = (B_2-B_1)/B_2$; and $\lambda^2 = 1-\beta^2$. The mirror-modified distribution function $f_1(\mathbf{v})$ has an electron density that differs slightly from the core-halo model total density, η. The corrections to the core-halo contribution to the electron density represent the nonlocal mirroring signatures of the approaching shock layer discussed above. It is clear from (A2) that η is only synonymous with N_{e1} in the limit $\beta^2 \to 0$, where the shock strength vanishes. The inferred number of reflected electrons depends on the size of the cross-shock potential as embedded in ϕ and the sonic Mach number of the shock ν.

A2. Upstream Electron Bulk Speed

In the HTF the upstream electron bulk speed is parallel to the upstream magnetic field and is obtained by setting $\mathcal{H}(\mathbf{v}_1) = v_{1||}$ in (A1) and dividing by the electron density, which gives

$$U_{e1||}(\psi,\phi,\nu) = \frac{\eta\psi}{N_{e1}}(1-\delta)\left(1-\beta^3 e^{-\xi_c^2}\right) + \frac{\eta\psi}{N_{e1}}\delta\left(1-\beta^3 e^{-\xi_h^2}\right). \qquad \text{(A5)}$$

As a cross check of the functional form of $U_{e1||}$, we immediately see that $\psi = U_{e1||}$ when the upcoming shock disappears ($\beta^2 \to 0$) as expected. A closer inspection of (A5) reveals that the net effect of electron mirroring ($\beta^2 \neq 0$) is to reduce the unperturbed solar wind bulk speed, ψ. Moreover, (A5) can be inverted using (A2) to yield ψ as a function of ϕ and ν given the upstream bulk speed:

$$\psi = \frac{U_{e1||}(1-\delta)[1+\beta e^{-\xi_c^2}\mathrm{erf}(\beta\nu)]}{\left\{(1-\delta)\left(1-\beta^3 e^{-\xi_c^2}\right)+\delta\left(1-\beta^3 e^{-\xi_h^2}\right)\right\}} + \frac{U_{e1||}\delta[1+\beta e^{-\xi_h^2}\mathrm{erf}(\frac{\beta\nu}{\gamma})]\Big\}}{\left\{(1-\delta)\left(1-\beta^3 e^{-\xi_c^2}\right)+\delta\left(1-\beta^3 e^{-\xi_h^2}\right)\right\}}. \qquad \text{(A6)}$$

A3. Upstream Electron Pressure

The upstream pressure tensor is gyrotropic and is given by the following expression:

$$\mathbf{P_{e1}} = P_{1||}\hat{\mathbf{b}}\hat{\mathbf{b}} + P_{1\perp}(I - \hat{\mathbf{b}}\hat{\mathbf{b}}), \tag{A7}$$

where I is the unit tensor and $\hat{\mathbf{b}}$ is the magnetic field unit vector. The parallel contribution to the upstream random electron pressure is given by

$$P_{1||} = \Pi_{e1||} - m_e N_{e1} {U_{e1||}}^2, \tag{A8}$$

where the dynamic pressure $\Pi_{e1||}$ is obtained from (A1) by setting $\mathcal{H}(\mathbf{v}_1) = {v_{1||}}^2$ and multiplying by m_e which leads to the following relation

$$\begin{aligned}\Pi_{e1||} &= m_e\eta(1-\delta)\left(\frac{\psi}{\nu}\right)^2\left\{\frac{1}{2}+\nu^2\right.\\ &\left.+\left[\beta^4\nu\exp(-\beta^2\nu^2)+\left(\frac{\beta^3}{2}+\beta^5\nu^2\right)\mathrm{erf}(\beta\nu)\right]e^{-\xi_c^2}\right\}\\ &+ m_e\eta\delta\left(\frac{\gamma\psi}{\nu}\right)^2\left\{\frac{1}{2}+\frac{\nu^2}{\gamma^2}+\left[\frac{\beta^4\nu}{\gamma}\exp\left(-\frac{\beta^2\nu^2}{\gamma^2}\right)\right.\right.\\ &\left.\left.+\left(\frac{\beta^3}{2}+\frac{\beta^5\nu^2}{\gamma^2}\right)\mathrm{erf}\left(\frac{\beta\nu}{\gamma}\right)\right]e^{-\xi_c^2}\right\}.\end{aligned} \tag{A9}$$

Assigning $\mathcal{H}(\mathbf{v}_1) = {v_{1\perp}}^2$ in (A1) and multiplying by $m_e/2$ yields the perpendicular contribution to the electron pressure given by

$$\begin{aligned}P_{1\perp} &= \frac{m_e\eta(1-\delta)\psi^2}{2\nu^2}\left\{1+\frac{\nu\beta^2\lambda^2}{\sqrt{\pi}}\exp\left[-\beta^2\nu^2\right]e^{-\xi_c^2}\right.\\ &\left.+\beta\mathrm{erf}\left(\beta\nu\right)\left(1+\frac{\lambda^2}{2}+\frac{\phi^2}{\alpha^2}+\beta^2\nu^2\lambda^2\right)e^{-\xi_c^2}\right\}\\ &+\frac{m_e\eta\delta\gamma^2\psi^2}{2\nu^2}\left\{1+\frac{\nu\beta^2\lambda^2}{\sqrt{\pi}\gamma}\exp\left[-\frac{\beta^2\nu^2}{\gamma^2}\right]e^{-\xi_h^2}\right.\\ &\left.+\beta\mathrm{erf}\left(\frac{\beta\nu}{\gamma}\right)\left(1+\frac{\lambda^2}{2}+\frac{\phi^2}{\alpha^2\gamma^2}+\frac{\beta^2\nu^2\lambda^2}{\gamma^2}\right)e^{-\xi_h^2}\right\}.\end{aligned} \tag{A10}$$

The upstream temperature T_{e1} is obtained by the following:

$$T_{e1} = \frac{P_{1||} + 2P_{1\perp}}{N_{e1}}. \tag{A11}$$

Appendix B: Downstream Electron Moments

A similar set of expressions in terms of the shape parameters can be obtained by taking velocity moments of the downstream distribution function f_2. In addition to contributions to f_2 from electron orbits that connect to the upstream side of the shock, there may be contributions to these moments from electron orbits having origins farther downstream of the shock that connect to the region inaccessible from the upstream boundary, and/or that can not access either boundary. These three classes of characteristic curves are well known in solutions of partial differential equations by the method of characteristics [e.g., *Morse and Feshbach*, 1953]. The need to specify a nonvanishing electron distribution function (e.g., $A \neq 0$) in the ellipsoidal region is discussed in section 2.4. In general, the odd moments of the downstream electron distribution function determined in the shock rest frame, such as the number flux or energy flux, are independent of the functional form of ${f_2}^{\mathrm{ellipse}}$ because the distribution function in this region must be mirror symmetric, whereas the even moments such as the density and electron pressure will be dependent. These contributions will be denoted by using the superscript "ellipse" in the moment equations below.

Evaluation of the downstream moments over downstream velocity space determined by the V-L mapping is complex because of the ellipsoidal boundary (as in Figure 2b). Transforming to upstream velocity space variables dramatically simplifies the calculations. Thus, in computing the mapped contribution to the downstream electron moments we use integrals of the form

$$\begin{aligned}\int d^3\mathbf{v}_2 {f_2}^{\mathrm{V-L}}(\mathbf{v}_2)\mathcal{H}(\mathbf{v}_2) \equiv \int d^3\mathbf{v}_1 \left|\frac{\delta\mathbf{v}_2}{\delta\mathbf{v}_1}\right|\\ \times f_1[\mathbf{v}_1(\mathbf{v}_2)]\mathcal{H}[\mathbf{v}_2(\mathbf{v}_1)],\end{aligned} \tag{B1}$$

where $\mathcal{H}[\mathbf{v}_2(\mathbf{v}_1)]$ is a function of the upstream velocity through the conservation of energy and magnetic moment relations. In (B1), Liouville's theorem was used to write ${f_2}^{\mathrm{V-L}}(\mathbf{v}_2)$ as the same functional value at the other boundary, $f_1[\mathbf{v}_1(\mathbf{v}_2)]$. The magnitude of the determinant of the Jacobian matrix, determined from (6), is given by

$$\left|\frac{\delta\mathbf{v}_2}{\delta\mathbf{v}_1}\right| = \left(\frac{\alpha}{\beta}\right)^2 \frac{|v_{1||}|}{\sqrt{{v_{1||}}^2 + {v_\Phi}^2 - \alpha^2{v_{1\perp}}^2}}. \tag{B2}$$

B1. Downstream Electron Density

The downstream density is given by the following expression:

$$\begin{aligned}N_{e2} &= \eta(1-\delta)\left(\frac{\alpha}{\beta}\right)^2\frac{2}{\sqrt{\pi}}\int_{-\infty}^{\infty}d\tau\exp\left[-\left(\tau-\nu\right)^2\right]\\ &\times\left(\frac{\tau^2}{\tau^2+\phi^2}\right)^{\frac{1}{2}}\Delta(\chi_{+c})\\ &+\eta\delta\left(\frac{\alpha}{\beta}\right)^2\frac{2}{\sqrt{\pi}}\int_{-\infty}^{\infty}d\tau\exp\left[-\left(\tau-\frac{\nu}{\gamma}\right)^2\right]\\ &\times\left(\frac{\tau^2}{\tau^2+\frac{\phi^2}{\gamma^2}}\right)^{\frac{1}{2}}\Delta(\chi_{+h})\\ &+ {N_{e2}}^{\mathrm{ellipse}},\end{aligned} \tag{B3}$$

where $\Delta(x)$, related to Dawson's integral, is defined as

$$\Delta(x) \equiv x\exp\left(-x^2\right)\int_0^x ds\exp\left(s^2\right). \tag{B4}$$

The χ_{+c} and χ_{+h} are given by

$$\chi_{+c}(\tau) \equiv \sqrt{\frac{\left(\tau^2+\phi^2\right)}{\alpha^2}}, \tag{B5}$$

$$\chi_{+h}(\tau) \equiv \sqrt{\frac{\left(\tau^2+(\phi/\gamma)^2\right)}{\alpha^2}}. \tag{B6}$$

In (B3), ${N_{e2}}^{\text{ellipse}}$ given by

$$\begin{aligned} {N_{e2}}^{\text{ellipse}} &= \frac{4A\eta\phi^3}{3\sqrt{\pi}\beta^2}\Big[(1-\delta)\exp\left(-\nu^2\right) \\ &\quad + \frac{\delta}{\gamma^3}\exp\left(-\frac{\nu^2}{\gamma^2}\right)\Big] \end{aligned} \tag{B7}$$

represents possible contributions to the downstream distribution function from electrons farther downstream in the magnetosheath that have access to the ellipsoid region (as in Figure 2b) but do not have access to the upstream side of the shock.

B2. Downstream Electron Bulk Speed

The downstream electron bulk speed is trivially related to the upstream electron bulk speed through the steady state continuity equation for electrons and is given by the following expression:

$$U_{e2||} = \frac{N_{e1}}{N_{e2}}\left(\frac{\alpha}{\beta}\right)^2 U_{e1||} \equiv \frac{N_{e1}U_{e1||}}{B_1}\frac{B_2}{N_{e2}}. \tag{B8}$$

The ellipsoid contribution enters here only through N_{e2}.

B3. Downstream Electron Pressure

The downstream pressure tensor is defined by the following expression:

$$\mathbf{P_{e2}} = P_{2||}\hat{\mathbf{b}}\hat{\mathbf{b}} + P_{2\perp}(I - \hat{\mathbf{b}}\hat{\mathbf{b}}), \tag{B9}$$

where I is the unit tensor and $\hat{\mathbf{b}}$ is the magnetic field unit vector. The parallel contribution to the downstream electron pressure is defined as

$$P_{2||} = \Pi_{e2||} - m_e N_{e2} {U_{e2||}}^2. \tag{B10}$$

$\Pi_{e2||}$ is obtained from (B1) by setting $\mathcal{H}[\mathbf{v_2}(\mathbf{v_1})] = {v_{2||}}^2(v_{1||}, v_{1\perp})$ and multiplying by m_e, which leads to the following relation:

$$\begin{aligned} \Pi_{e2||} &= \frac{m_e\eta}{\sqrt{\pi}}(1-\delta)\left(\frac{\alpha\psi}{\beta\nu}\right)^2\int_{-\infty}^{\infty}d\tau\exp\left[-(\tau-\nu)^2\right] \\ &\quad\times\left\{|\tau|\left(\tau^2+\phi^2\right)^{\frac{1}{2}} - \alpha^2\left(\frac{\tau^2}{\tau^2+\phi^2}\right)^{\frac{1}{2}}\Delta(\chi_{+c})\right\} \\ &\quad + \frac{m_e\eta}{\sqrt{\pi}}\delta\left(\frac{\alpha\gamma\psi}{\beta\nu}\right)^2\int_{-\infty}^{\infty}d\tau\exp\left[-\left(\tau-\frac{\nu}{\gamma}\right)^2\right] \\ &\quad\times\left\{|\tau|\left(\tau^2+\frac{\phi^2}{\gamma}\right)^{\frac{1}{2}} - \alpha^2\left(\frac{\tau^2}{\tau^2+\frac{\phi^2}{\gamma}}\right)^{\frac{1}{2}}\Delta(\chi_{+h})\right\} \\ &\quad + \Pi_{e2||}^{\text{ellipse}}, \end{aligned} \tag{B11}$$

where the ellipsoid contribution to the parallel pressure $\Pi_{e2||}^{\text{ellipse}}$ is given by

$$\begin{aligned} \Pi_{e2||}^{\text{ellipse}} &= \frac{4m_eA\eta\phi^5}{15\sqrt{\pi}\beta^2}\left(\frac{\psi}{\nu}\right)^2\Big[(1-\delta)\exp(-\nu^2) \\ &\quad + \frac{\delta}{\gamma^3}\exp(-\frac{\nu^2}{\gamma^2})\Big]. \end{aligned} \tag{B12}$$

The perpendicular contribution to the pressure tensor is obtained by setting $\mathcal{H}[\mathbf{v_2}(\mathbf{v_1})] = {v_{2\perp}}^2(v_{1||}, v_\perp)$ in (B1) and multiplying by $m_e/2$, which results in the following expression:

$$\begin{aligned} P_{2\perp} &= \frac{m_e\eta(1-\delta)}{\sqrt{\pi}}\left(\frac{\alpha^2\psi}{\beta^2\nu}\right)^2\int_{-\infty}^{\infty}d\tau\exp[-(\tau-\nu)^2] \\ &\quad\times\left(\frac{\tau^2}{\tau^2+\phi^2}\right)^{\frac{1}{2}}\left[\Psi(\chi_{+c}) + \frac{\Delta(\chi_{+c})}{2}\right] \\ &\quad + \frac{m_e\eta\delta}{\sqrt{\pi}}\left(\frac{\alpha^2\gamma\psi}{\beta^2\nu}\right)^2\int_{-\infty}^{\infty}d\tau\exp\left[-\left(\tau-\frac{\nu}{\gamma}\right)^2\right] \\ &\quad\times\left(\frac{\tau^2}{\tau^2+\frac{\phi^2}{\gamma}}\right)^{\frac{1}{2}}\left[\Psi(\chi_{+h}) + \frac{\Delta(\chi_{+h})}{2}\right] \\ &\quad + P_{2\perp}^{\text{ellipse}}, \end{aligned} \tag{B13}$$

where $\Psi(x)$ is given in terms of Dawson's integral by the relation $\Psi(x) = x^2[\Delta(x) - 1/2]$. The ellipsoid contribution $P_{2\perp}^{\text{ellipse}}$ is represented by

$$\begin{aligned} P_{2\perp}^{\text{ellipse}} &= \frac{4m_eA\eta\phi^5}{15\sqrt{\pi}\beta^4}\left(\frac{\psi}{\nu}\right)^2\Big[(1-\delta)\exp(-\nu^2) \\ &\quad + \frac{\delta}{\gamma^3}\exp\left(-\frac{\nu^2}{\gamma^2}\right)\Big]. \end{aligned} \tag{B14}$$

The downstream temperature T_{e2} is obtained by the following:

$$T_{e2} = \frac{P_{2||} + 2P_{2\perp}}{3N_{e2}}. \tag{B15}$$

Acknowledgments. We would like to acknowledge the roles played in the design of the ISEE VES by K. W. Ogilvie and archival and analysis support by R. J. Fitzenreiter, both of NASA's GSFC. We also acknowledge M. Thomsen of the Los Alamos National Laboratory for providing us with the ion moment data used in this study. Support for this research for A. J. H. was provided by the GSRP fellowship program under the NASA grant NGT-70411.

Michel Blanc thanks the two referees for their assistance in evaluating this paper.

References

Balikhin, M., V. V. Krasnosel'skikh, L. J. C. Woolliscroft, and M. Gedalin, A study of the dispersion of the electron distribution in the presence of E and B gradients: Application to electron heating at quasi-perpendicular shocks, *J. Geophys. Res.*, *103*, 2029–2040, 1998.

Bame, S. J., J. R. Asbridge, H. E. Felthauser, J. P. Glore, G. Paschmann, P. Hemmerich, K. Lehmann, and H. Rosenbauer, ISEE-1 and ISEE-2 fast plasma experi-

ment and the ISEE-1 solar wind experiment, *IEEE Trans. Geosci. Electron.*, *16*(3), 216–220, 1978.

Biskamp, D., Collisionless shock waves in plasmas, *Nucl. Fusion*, *13*, 719–740, 1973.

Boyd, T. J. M., and J. J. Sanderson, *Plasma Dynamics*, Barnes and Noble, New York, 1969.

Burgess, D., W. P. Wilkinson, and S. J. Schwartz, Ion distributions and thermalization at perpendicular and quasi-perpendicular supercritical collisionless shocks, *J. Geophys. Res.*, *94*, 8783–8792, 1989.

Feldman, W. C., Electron velocity distributions near collisionless shocks, in *Collisionless Shocks in the Heliosphere: Reviews of Current Research*, *Geophys. Monogr. Ser.*, vol. 35, edited by B. T. Tsurutani and R. G. Stone, pp. 195–205, AGU, Washington, D. C., 1985.

Feldman, W. C., J. R. Asbridge, S. J. Bame, M. D. Montgomery, and S. P. Gary, Solar wind electrons, *J. Geophys. Res.*, *80*, 4181–4196, 1975.

Feldman, W. C., R. C. Anderson, S. J. Bame, J. T. Gosling, R. D. Zwickl, and E. J. Smith, Electron velocity distributions near interplanetary shocks, *J. Geophys. Res.*, *88*, 9949–9958, 1983a.

Feldman, W. C., S. J. Bame, S. P. Gary, J. T. Gosling, D. J. McComas, M. F. Thomsen, G. Paschmann, and M. M. Hoppe, Electron velocity distributions near the Earth's bow shock, *J. Geophys. Res.*, *88*, 96–110, 1983b.

Fitzenreiter, R. J., The electron foreshock, *Adv. Space Res.*, *15*(8/9), 9–27, 1995.

Fitzenreiter, R. J., J. D. Scudder, and A. J. Klimas, Three-dimensional analytical model for the spatial variation of the foreshock electron distribution function: Systematics and comparisons with ISEE observations, *J. Geophys. Res.*, *95*, 4155–4173, 1990.

Goodrich, C. C., Numerical simulations of quasi-perpendicular collisionless shocks, in *Collisionless Shocks in the Heliosphere: Reviews of Current Research*, *Geophys. Monogr. Ser.*, vol. 35, edited by B. T. Tsurutani and R. G. Stone, pp. 153–168, AGU, Washington, D. C., 1985.

Goodrich, C. C., and J. D. Scudder, The adiabatic energy change of plasma electrons and the frame dependence of the cross-shock potential at collisionless magnetosonic shock waves, *J. Geophys. Res.*, *89*, 6654–6662, 1984.

Gosling, J. T., and A. E. Robson, Ion reflection, gyration, and dissipation at supercritical shocks, in *Collisionless Shocks in the Heliosphere: Reviews of Current Research*, *Geophys. Monogr. Ser.*, vol. 35, edited by B. T. Tsurutani and R. G. Stone, pp. 141–152, AGU, Washington, D. C., 1985.

Hull, A. J., Partition of temperature between electrons and ions across collisionless, fast mode shocks, Ph.D. thesis, Univ. of Iowa, Iowa City, 1998.

Hull, A. J., J. D. Scudder, L. A. Frank, W. R. Paterson, R. J. Fitzenreiter, C. T. Russell, S. Kokubun, and T. Yamamoto, Coherent electron heating and phase space signatures at strong shocks (abstract), *Eos Trans. AGU*, *78*(17), Spring Meet. Suppl., S281, 1997.

Hull, A. J., J. D. Scudder, L. A. Frank, W. R. Paterson, and M. G. Kivelson, Electron heating and phase space signatures at strong and weak quasi-perpendicular shocks, *J. Geophys. Res.*, *103*, 2041–2054, 1998.

Hull, A. J., J. D. Scudder, R. J. Fitzenreiter, K. W. Ogilvie, J. A. Newbury, and C. T. Russell, Electron temperature and de Hoffmann-Teller potential change across the Earth's bow shock: New results from ISEE 1, *J. Geophys. Res.*, *105*, 20,957–20,971, 2000.

Klimas, A. J., The electron foreshock, in *Collisionless Shocks in the Heliosphere: Reviews of Current Research*, *Geophys. Monogr. Ser.*, vol. 35, edited by B. T. Tsurutani and R. G. Stone, pp. 237–252, AGU, Washington, D. C., 1985.

Krauss-Varban, D., F. G. E. Pantellini, and D. Burgess, Electron dynamics and whistler waves at quasi-perpendicular shocks, *Geophys. Res. Lett.*, *22*, 2091–2094, 1995.

Leroy, M. M., and D. Winske, Backstreaming ions from oblique Earth bow shocks, *Ann. Geophys.*, *1*, 527–536, 1983.

Leroy, M. M., D. Winske, C. C. Goodrich, C. S. Wu, and K. Papadopoulos, The structure of perpendicular bow shocks, *J. Geophys. Res.*, *87*, 5081–5094, 1982.

McKean, M. E., N. Omidi, D. Krauss-Varban, and H. Karimabadi, Wave and particle evolution downstream of quasi-perpendicular shocks, *Adv. Space Res.*, *15*(8/9), 319–322, 1995.

Montgomery, M. D., J. R. Asbridge, and S. J. Bame, Vela 4 plasma observations near the Earth's bow shock, *J. Geophys. Res.*, *75*, 1217–1230, 1970.

Morawetz, C. S., Magnetohydrodynamic shock structure without collisions, *Phys. Fluids*, *4*, 988–1006, 1961.

Morawetz, C. S., Modification for magnetohydrodynamic shock structure without collisions, *Phys. Fluids*, *5*, 1447–450, 1962.

Morse, P. M., and H. Feshbach, *Methods of Theoretical Physics*, vol. 1, McGraw-Hill, New York, 1953.

Newbury, J. A., C. T. Russell, and M. Gedalin, The ramp widths of high-Mach-number, quasi-perpendicular collisionless shocks, *J. Geophys. Res.*, *103*, 29,581–29,593, 1998.

Ogilvie, K. W., J. D. Scudder, and H. Doong, The electron spectrometer experiment on ISEE-1, *IEEE Trans. Geosci. Electron.*, *16*(3), 261–265, 1978.

Paschmann, G., N. Sckopke, S. J. Bame, and J. T. Gosling, Observations of gyrating ions in the foot of the nearly perpendicular bow shock, *Geophys. Res. Lett.*, *9*, 881–884, 1982.

Russell, C. T., M. M. Hoppe, W. A. Livesey, J. T. Gosling, and S. J. Bame, ISEE 1-2 observations of laminar bow shocks: Velocity and thickness, *Geophys. Res. Lett.*, *9*, 1171–1174, 1982.

Sagdeev, R. Z., Cooperative phenomena and shock waves in collisionless plasmas, in *Reviews of Plasma Physics*, vol. 4, edited by M. A. Leontovich, pp. 23–91, Consult. Bur., New York, 1966.

Savoini, P., and B. Lembege, Electron dynamics in two and one dimensional oblique supercritical collisionless magnetosonic shocks, *J. Geophys. Res.*, *99*, 6609–6635, 1994.

Schwartz, S. J., M. F. Thomsen, W. C. Feldman, and F. T. Douglas, Electron heating and potential jump across slow mode shocks, *J. Geophys. Res.*, *92*, 3165–3174, 1987.

Schwartz, S. J., M. F. Thomsen, S. J. Bame, and J. T. Stansberry, Electron heating and the potential jump across fast mode shocks, *J. Geophys. Res.*, *93*, 12,923–12,931, 1988.

Sckopke, N., G. Paschmann, S. J. Bame, J. T. Gosling, and C. T. Russell, Evolution of ion distributions across the nearly perpendicular bow shock: Specularly and non-specularly reflected-gyrating ions, *J. Geophys. Res.*, *88*, 6121–6136, 1983.

Sckopke, N., G. Paschmann, A. L. Brinca, C. W. Carlson, and H. Lühr, Ion thermalization in quasi-perpendicular shocks involving reflected ions, *J. Geophys. Res.*, *95*, 6337–6352, 1990.

Scudder, J. D., The field-aligned flow approximation for electrons within layers possessing a normal mass flux: A corollary to the deHoffmann-Teller theorem, *J. Geophys. Res.*, *92*, 13,447–13,455, 1987.

Scudder, J. D., A review of the physics of electron heating

at collisionless shocks, *Adv. Space Res.*, *15*(8/9), 181–223, 1995.

Scudder, J. D., D. L. Lind, and K. W. Ogilvie, Electron observations in the solar wind and magnetosheath, *J. Geophys. Res.*, *78*, 6535–6548, 1973.

Scudder, J. D., A. Mangeney, C. Lacombe, C. C. Harvey, T. L. Aggson, R. Anderson, J. T. Gosling, G. Paschmann, and C. T. Russell, The resolved layer of a collisionless, high β, supercritical, quasi-perpendicular shock wave, 1, Rankine-Hugoniot geometry, currents, and stationarity, *J. Geophys. Res.*, *91*, 11,019–11,052, 1986a.

Scudder, J. D., A. Mangeney, C. Lacombe, C. C. Harvey, and T. L. Aggson, The resolved layer of a collisionless, high β, supercritical, quasi-perpendicular shock wave, 2, Dissipative fluid electrodynamics, *J. Geophys. Res.*, *91*, 11,053–11,073, 1986b.

Scudder, J. D., A. Mangeney, C. Lacombe, C. C. Harvey, C. Wu, and R. Anderson, The resolved layer of a collisionless, high β, supercritical, quasi-perpendicular shock wave, 3, Vlasov electrodynamics, *J. Geophys. Res.*, *91*, 11,074–11,097, 1986c.

Thomsen, M. F., M. M. Mellott, J. A. Stansberry, S. J. Bame, J. T. Gosling, and C. T. Russell, Strong electron heating at the Earth's bow shock, *J. Geophys. Res.*, *92*, 10,119–10,124, 1987.

Viñas, A. F., and J. D. Scudder, Fast and optimal solution to the Rankine-Hugoniot problem, *J. Geophys. Res.*, *91*, 39–58, 1986.

Whang, Y. C., Slow shocks and their transition to fast shocks in the inner solar wind, *J. Geophys. Res.*, *92*, 4349–4356, 1987.

Wilkinson, W. P., Ion kinetic processes and thermalization at quasi-perpendicular low Mach number shocks, *J. Geophys. Res.*, *96*, 17,675–17,688, 1991.

Winske, D., M. Tanaka, C. S. Wu, and K. B. Quest, Plasma heating at collisionless shocks due to the kinetic cross-field streaming instability, *J. Geophys. Res.*, *90*, 123–136, 1985.

Wu, C. S., et al., Microinstabilities associated with a high Mach number, perpendicular shock, *Space Sci. Rev.*, *37*, 63–109, 1984.

A. J. Hull, Space Science Laboratory, University of California, Berkeley, CA 94720. (ahull@ssl.berkeley.edu)

J. D. Scudder, Department of Physics and Astronomy, University of Iowa, Iowa City, IA 52242. (jds@hydra.physics.uiowa.edu)

(Received August 30, 1999; revised April 19, 2000; accepted June 25, 2000.)